

## Thermal-neutron capture by $^{14}\text{N}$

E. T. Jurney, J. W. Starner, and J. E. Lynn  
*Los Alamos National Laboratory, Los Alamos, New Mexico 87545*

S. Raman  
*Oak Ridge National Laboratory, Oak Ridge, Tennessee 37831*  
 (Received 5 February 1997)

The energies and intensities of 58  $\gamma$  rays emitted in thermal-neutron capture by nitrogen (99.63%  $^{14}\text{N}$ ) have been measured accurately. A major reason was to establish this reaction as a standard for similar measurements on other nuclides. These  $\gamma$  rays have been placed between 19 known levels (including the ground state and the capturing state) in  $^{15}\text{N}$ . The primary  $\gamma$  rays of both electric dipole ( $E1$ ) and magnetic dipole ( $M1$ ) types have been analyzed with existing theories of slow-neutron capture. Unlike many other light nuclides, the cross sections for  $E1$  transitions in  $^{15}\text{N}$  differ drastically from the calculations of pure direct-capture theory. The role of the resonance-capture contribution from the proton-unbound, neutron-bound level at  $29 \pm 2$  keV below the neutron separation energy was considered. Some of the properties of this level are quite well known from the  $^{14}\text{C}(p, \gamma)$  reaction, and others can be derived from an  $\mathcal{R}$ -matrix analysis of the total cross section as a function of neutron energy. The thermal-neutron capture  $\gamma$ -ray spectrum is different from the proton-capture  $\gamma$ -ray spectrum, but if proper account is taken of the interference among the compound-nuclear processes, the valence-neutron mechanism, and potential capture, the data can be satisfactorily explained. In the thermal-neutron reaction, compound-nuclear  $E1$  and direct-capture  $E1$  contributions are of comparable magnitude. Valence-neutron capture forms a significant component of capture by the neutron-bound level at  $-29$  keV. Largely destructive interference between compound-nuclear and valence processes in a few transitions in thermal-neutron capture gives rise to a much smaller total cross section than would be obtained from the compound-nuclear process alone. The  $M1$  transitions also show some evidence of a direct process but not a dominant one. The magnitudes of the compound-nuclear transitions, both  $E1$  and  $M1$ , are largely consistent with the values implied by giant resonance theories. The resonance parameters deduced for the  $-29$ -keV level are: total radiation width =  $565 \pm 24$  meV, reduced neutron width =  $51.6 \pm 0.3$  keV (for a channel radius of 3.5 fm), and proton width =  $160 \pm 30$  meV. [S0556-2813(97)02607-1]

PACS number(s): 25.40.Lw, 23.20.Lv, 27.20.+n

### I. INTRODUCTION

Studies of  $\gamma$  rays following thermal-neutron capture by light ( $A < 50$ ) nuclides have shown that the mechanism predominantly responsible for producing primary electric-dipole ( $E1$ ) transitions is the direct one [1]. In recent works [2–15] the direct (thermal  $n, \gamma$ ) reaction has been treated within a realistic optical-model framework, thus allowing precise comparisons between theory and data. At the same time, the accuracy and sensitivity of experimental methods for determining the cross sections of transitions to individual final states have greatly improved.

In the  $0p$  shell, the nuclides treated previously are  $^7\text{Li}$ ,  $^9\text{Be}$ ,  $^{12}\text{C}$ , and  $^{13}\text{C}$  [4,8,9]. The cross sections of primary  $E1$  transitions agree with direct-capture theory despite the fact that the neutron-scattering lengths are often so large (compared to the potential scattering length) that they adversely affect our ability to calculate these cross sections. In the light of the pattern so far revealed, it is interesting to study the target nucleus  $^{14}_7\text{N}_7$  (spin and parity  $1^+$ ), which also has a particularly large neutron scattering length. The fact that  $^{14}\text{N}$  has only one neutron short of closure of the  $0p$  shell has consequences not only of bringing remnants of the  $0p$  strength close to the ground state of  $^{15}\text{N}$ , but also of

giving this nucleus high enough energy in its initial capturing state such that primary magnetic-dipole ( $M1$ ) transitions can proceed to a considerable number of bound positive-parity states arising from the  $1s0d$  shell. Whether a direct mechanism plays any role in governing the strength of  $M1$  transitions may therefore also be addressed.

It is interesting to investigate the  $^{14}\text{N}$  (thermal  $n, \gamma$ ) reaction also because it has been our canonical energy and intensity standard since 1961 when the special advantages of this reaction, using melamine ( $\text{C}_3\text{H}_6\text{N}_6$ ) as target material, was exploited by Motz, Carter, and Barfield [16]. Subsequently, nearly all laboratories that are engaged in ( $n, \gamma$ ) measurements [17–25] have directly or indirectly used this standard.

The measurements are described in Sec. II. Application of the capture theory requires a knowledge of ( $d, p$ ) spectroscopic factors, neutron-scattering lengths, and resonance parameters, all of which are discussed in Sec. III. Comparisons of the calculated cross sections of primary  $E1$  and  $M1$  transitions with measurements are described in Sec. IV and Sec. V, respectively. Contrary to our expectations from previous studies within the  $0p$  shell, the calculated direct-capture  $E1$  transition strengths are very different from the measured

values.<sup>1</sup> The latter values are also very different from what one may call the compound-nuclear expectations, which can be deduced from investigations of the  $^{14}\text{C}(p, \gamma)$  reaction [26–33]. [The proton separation energy  $S_p(^{15}\text{N}) = 10\,207.4$  keV is close to (but lower than) the neutron separation energy  $S_n(^{15}\text{N}) = 10\,833.3$  keV.] Indeed, early measurements by Bartholomew *et al.* [26] showed that the  $\gamma$ -ray spectra from the proton resonances below and near the neutron threshold are very different from the (thermal  $n, \gamma$ ) spectrum. These observations have not been satisfactorily explained for over four decades. It now appears that there is a remarkable interplay between the resonance (compound-nuclear) contributions on the one hand and the valence- and the potential-capture components of direct capture on the other; these combine in a largely destructive fashion leaving neither the (thermal  $n, \gamma$ ) spectrum nor the near-neutron-threshold ( $p, \gamma$ ) spectrum having the characteristics that are typical of either the direct or compound-nuclear picture. The resonance ( $p, \gamma$ ) spectrum can be interpreted, in fact, to show the strong influence of the neutron-valence mechanism. This joint analysis of thermal-neutron capture and proton capture is described in Sec. VI. Our conclusions are summarized in Sec. VII.

A number of primary  $M1$  transitions with cross sections as great as those of primary  $E1$  transitions exist in  $^{15}\text{N}$ . It has been speculated elsewhere [10] that a direct  $M1$  mechanism analogous to the direct  $E1$  process may play a significant role in thermal-neutron capture by light nuclides. The analysis of the  $^{15}\text{N}$  data presented in Sec. V leads to the conclusion that  $M1$  direct capture is playing only a minor role here in the capture process for low- to medium-energy transitions. This analysis also suggests that resonance  $M1$  capture as deduced from the ( $p, \gamma$ ) works [30,33] can explain the bulk of the  $M1$  transition strength.

## II. EXPERIMENTAL METHOD

### A. Capture facility

The  $^{14}\text{N}(n, \gamma)$  measurements with thermal neutrons were made at the internal target facility of the Los Alamos Omega West reactor utilizing 1750 mg of melamine in a high-purity graphite holder. This facility and the data analysis procedures have been described in Refs. [2,11]. The target was placed in a graphite holder, which was inside an evacuated bismuth channel. The target position was 1.5 m from the edge of the reactor core and at this position the thermal-neutron flux was nominally  $6 \times 10^{11}$  n/cm<sup>2</sup> s.  $\gamma$ -ray spectra were obtained with a 30-cm<sup>3</sup> coaxial intrinsic germanium detector positioned inside a 20-cm-diam $\times$ 30-cm-long NaI(Tl) annulus. This detector was located 6.3 m from the target and was operated either in the Compton-suppressed mode (0.3877 keV/channel) or in the pair-spectrometer mode

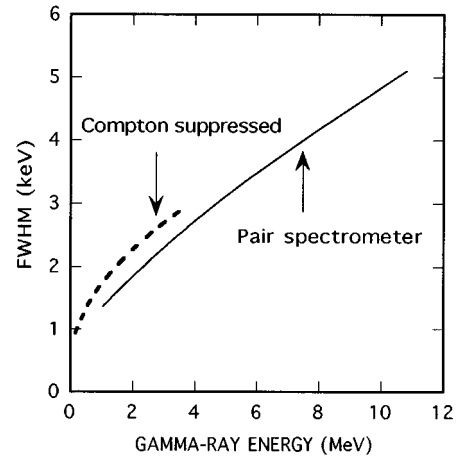


FIG. 1. Resolution [full width at half maximum (FWHM)] of our detection system.

(0.6285 keV/channel). The full width at half-maximum (FWHM) values for our system are shown in Fig. 1. In the pair-spectrometer mode, the FWHM values are 2.3, 3.1, 3.8, and 4.5 keV, respectively, for  $\gamma$ -ray energies of 3, 5, 7, and 9 MeV. At these energies, the resolution attained in the current study is better than that reported in all previous studies of the  $^{14}\text{N}(n, \gamma)$  reaction.

### B. Energy calibrations

In a particular energy region, the energy calibration requires two standards and a nonlinearity curve. Up to 3 MeV (in the Compton-suppressed mode), the standards traditionally used in our work are the  $510.999 \pm 0.001$  keV annihilation radiation and  $2223.253 \pm 0.004$  keV  $\gamma$  ray from the  $^1\text{H}(n, \gamma)$  reaction [34]. Because accurate energy standards are available in this energy region, the construction of a suitable nonlinearity curve (not shown) does not pose a serious problem. Between 1 and 13 MeV (in the pair-spectrometer mode) the standards employed invariably by us are the  $2223.253 \pm 0.004$  keV and  $4945.303 \pm 0.012$  keV  $\gamma$  rays from the  $^1\text{H}(n, \gamma)$  and  $^{12}\text{C}(n, \gamma)$  reactions, respectively [34]. These two are preferred because  $^1\text{H}$  is readily provided by the  $\text{CH}_2$  material used as a cross section standard and  $^{12}\text{C}$  by the graphite holder containing the target material, both in quantities sufficient to provide strong signals. Moreover, the former reaction generates just one  $\gamma$  ray and the latter just three strong  $\gamma$  rays. The problem of constructing an accurate nonlinearity curve in the high-energy region was again a lengthy process, for which several (thermal  $n, \gamma$ ) measurements were made, singly and in combinations, not only with melamine and  $\text{CH}_2$ , but also with  $\text{D}_2\text{O}$  and enriched  $^{13}\text{C}$ . The curve shown in Fig. 2 is based mainly on the  $\gamma$ -ray energies (in keV)  $2223.255 \pm 0.003$ ,  $4945.302 \pm 0.003$ , and  $6250.296 \pm 0.003$  deduced from the latest [35] neutron-separation energies (in keV)  $2224.5725 \pm 0.0022$ ,  $4946.3120 \pm 0.0023$ , and  $6257.2482 \pm 0.0024$ , for  $^2\text{D}$ ,  $^{13}\text{C}$ , and  $^3\text{T}$ , respectively, and on a value of  $3683.908 \pm 0.016$  keV deduced previously by us for the energy of a prominent  $\gamma$  ray from the  $^{12}\text{C}(n, \gamma)$  reaction. Because it is based on an extrapolation, the curve in Fig. 2 is less accurate above 6.3 MeV than in the 2.2–6.3-MeV region.

<sup>1</sup>In numerous compilations, F. Ajzenberg-Selove and T. Lauritsen [Nucl. Phys. **11**, 191 (1959)] and F. Ajzenberg-Selove [Nucl. Phys. **A152**, 117 (1970); **A268**, 137 (1976); **A360**, 129 (1981); **A449**, 127 (1986)] have implied that the experimental thermal-neutron capture cross section of  $^{14}\text{N}$  appears to be high relative to theoretical expectations. Actually it is *low*. Therein lies the problem.

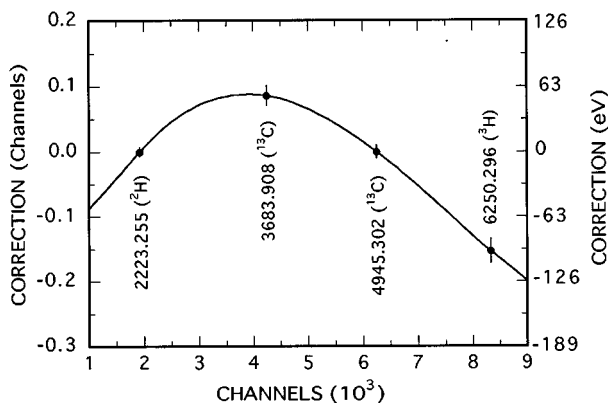


FIG. 2. Nonlinearity of our detection system.

### C. Intensity calibrations

Intensity calibrations were determined in the Compton-suppressed mode with a set of standard radioactive sources with precalibrated  $\gamma$ -ray intensities and were further checked with  $\gamma$  rays from  $^{82}\text{Br}$  decay [36,37] produced *in situ* in the internal target position. Between 200 and 3000 keV the curve shown in Fig. 3(a) is believed to be accurate to  $\sim 1\%$ . The efficiency curve in the pair-spectrometer mode [see Fig. 3(b)] was derived by a lengthy procedure. Convenient intensity standards (with  $\sim 1\%$  accuracies) that span the 3–11-MeV region do not exist. In fact, the reaction under study offers the best possibility of achieving such accuracies. Our starting point was the intensity values deduced from the  $^{14}\text{N}(n, \gamma)$  reaction by Motz, Carter, and Barfield [16] with a magnetic Compton spectrometer possessing a predictable efficiency curve. These values have been confirmed and refined by several authors (see discussion in Ref. [38]) such that by the middle 1980s it was possible to generate an efficiency curve with  $\sim 3\%$  accuracy in the 2–9-MeV region. Thermal ( $n, \gamma$ ) measurements were then made for over 20 nuclides lighter than the zinc isotopes. Some of these results have been published [11,13,15]. In the case of several light nuclides, the decay schemes are relatively simple and the intensity balance requirements (see Tables IV(A) and IV(B) of Ref. [11], Tables III(A) and III(C) of Ref. [13], and Table IV of Ref. [15]) can be used effectively to further refine and validate the efficiency curve. The resulting curve shown in Fig. 3(b) is believed to be accurate to  $\sim 1\%$  in the 2–7-MeV region,  $\sim 2\%$  in the 7–9-MeV region, and  $\sim 4\%$  in the 9–11-MeV region.

To obtain absolute cross sections using the relative efficiency curves of Figs. 3(a) and 3(b), a fiducial point is

needed. For this purpose, the 2223.3-keV  $\gamma$  ray from the  $^1\text{H}(n, \gamma)$  reaction is used. The results are cross checked using a value of  $0.452 \pm 0.009$  for the ratio of the intensities of the 1262-keV and 4946-keV  $\gamma$  rays from the  $^{12}\text{C}(n, \gamma)$  reaction. This value, determined in a previous experiment [39], is more precise than  $0.479 \pm 0.018$ , obtained in Ref. [40].

The capture cross sections reported in this work are based on measurements in which the melamine target was studied together with a 100.0-mg  $\text{CH}_2$  standard. The cross sections are normalized to the recommended value of  $\sigma_\gamma(2200 \text{ m/s}) = 332.6 \pm 0.7 \text{ mb}$  [41] for  $^1\text{H}$  present in this standard. The thermal-neutron flux at the target position approximates a Maxwellian distribution corresponding to a temperature of 350 K, for which the most probable neutron velocity is 2400 m/s. To determine the cross sections at 2200 m/s, a  $1/v$  dependence of the capture cross section is assumed for both  $^1\text{H}$  and  $^{14}\text{N}$ .

### D. $\gamma$ rays in $^{15}\text{N}$

Selected portions of the measured spectra are shown in Fig. 4. The energies and intensities of 58  $\gamma$  rays assigned to  $^{15}\text{N}$  are given in Table I. The weak ones, numbering about 30, are reported here for the first time. All of these  $\gamma$  rays have been incorporated into the level scheme given in Table II. The spin and parity ( $J^\pi$ ) values for all levels are known [42]. A primary transition has been observed to each of the 18 final states (16 bound and 2 proton-unbound) listed in Table II; of these 18 transitions, eight are  $E1$ , nine  $M1$ , and one  $E2$ . In addition to these 18 states, four other neutron-bound states ( $J^\pi$  in parentheses) are known [42] in  $^{15}\text{N}$  at 9829( $\frac{7}{2}^-$ ), 10 533( $\frac{5}{2}^+$ ), 10 693( $\frac{9}{2}^+$ ), and 10 804( $\frac{3}{2}^+$ ) keV. These four states are neither expected nor observed to be populated measurably in the  $^{14}\text{N}$  (thermal  $n, \gamma$ ) reaction. All levels listed in Table II are previously known, and the placements of transitions are consistent with existing data. The level energies listed in that table were obtained through an overall least-squares fit involving all transitions. In deducing these level energies, nuclear recoil was taken into account. The intensity balance for each of the excited states is good (see columns 4–6 of Table II).

The neutron separation energy ( $S_n$ ) of  $^{15}\text{N}$  was determined as  $10833.314 \pm 0.012 \text{ keV}$ . The best previously reported value from (thermal  $n, \gamma$ ) measurements is  $10 833.64 \pm 0.13 \text{ keV}$  [18]. Our value is in good agreement with  $10 833.3015 \pm 0.0024 \text{ keV}$ , which was deduced recently from a direct mass doublet measurement using a Penning trap [43].

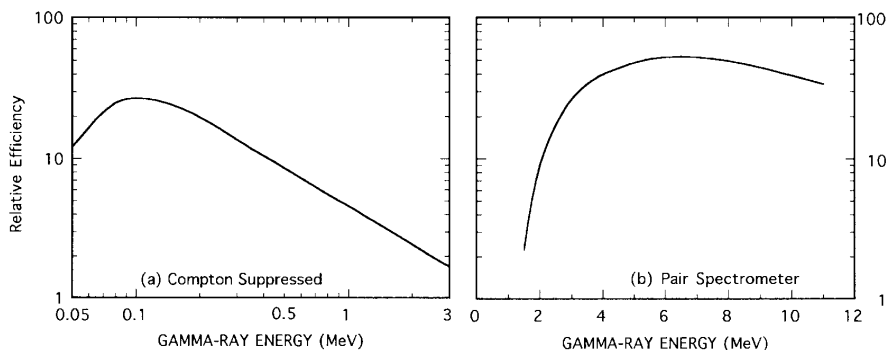


FIG. 3. Relative efficiency of our detection system.

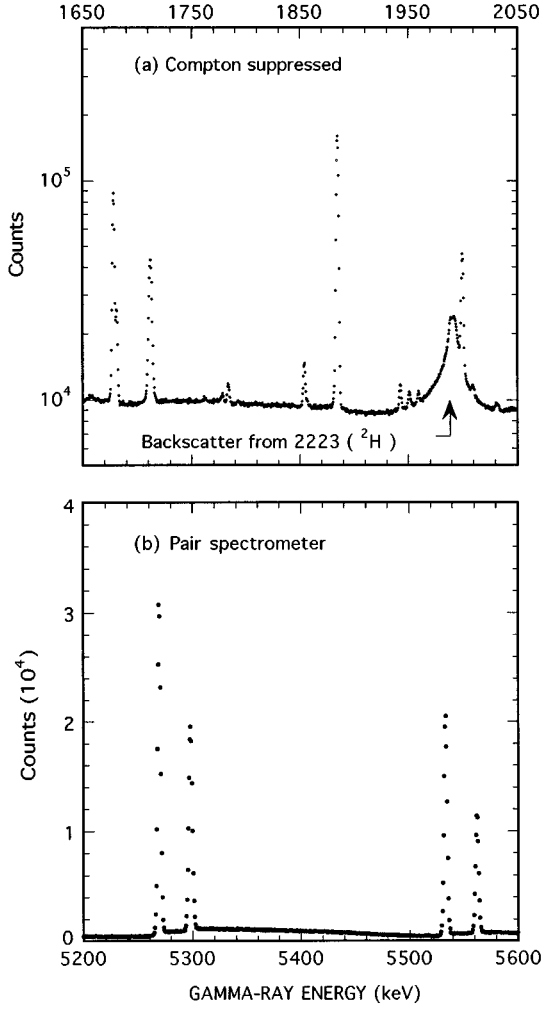


FIG. 4. Selected portions of the  $\gamma$ -ray spectrum from the  $^{14}\text{N}(n, \gamma)^{15}\text{N}$  reaction with thermal neutrons obtained using a melamine target.

If a level scheme is complete and internal conversion can be neglected, the quantities  $\Sigma I_\gamma$  (primary),  $\Sigma E_\gamma I_\gamma / S_n$ , and  $\Sigma I_\gamma$  (secondary to ground state) should all be the same within their stated uncertainties. In the case of  $^{15}\text{N}$ , the measured values (in units of mb) are  $79.8 \pm 0.7$ ,  $80.3 \pm 0.6$ , and  $80.9 \pm 0.6$ , respectively. Our recommended cross-section value of  $80.3 \pm 0.6$  mb is more precise than  $79.8 \pm 1.4$  mb obtained at McMaster [25].

The secondary ground-state transitions from the levels at 5299, 6324, 7301, and 8313 keV are measurably broadened as a result of recoil-induced Doppler broadening. The lifetime values deduced for these levels from an analysis of the  $\gamma$ -ray line shapes have been previously published [44].

### E. Secondary calibration standards

In Table III our measured energies and intensities for the strong  $\gamma$  rays observed in the  $^{14}\text{N}$  (thermal  $n, \gamma$ ) reaction have been compared with those obtained at McMaster [24]. Within the quoted uncertainties, these values overlap reasonably well.

## III. OTHER RELEVANT DATA

Within the direct-capture theory, the two crucial quantities entering the calculation of a partial cross section for a

particular primary  $\gamma$  ray are the final-state  $(d, p)$  spectroscopic strength and the (normally spin-dependent) neutron-scattering length. The measured  $(d, p)$  spectroscopic factors [45–47] are given in Table IV.

### A. Neutron-scattering lengths

The coherent scattering length and the total scattering cross section have been measured by Koester, Knopf, and Waschkowski [48] as  $a_{\text{coh}} = 8.74 \pm 0.02$  fm and  $\sigma_{\text{sc}} = 10.03 \pm 0.09$  b, respectively. The separate scattering lengths for the two spin states present in  $s$ -wave scattering can therefore be deduced as

$$a_{J=1/2} = 6.3 \pm 0.3 \text{ fm}, \quad a_{J=3/2} = 10.0 \pm 0.4 \text{ fm} \quad (1a)$$

or

$$a_{J=1/2} = 11.2 \pm 0.3 \text{ fm}, \quad a_{J=3/2} = 7.5 \pm 0.6 \text{ fm}. \quad (1b)$$

Evidence in favor of the first set comes from the resonances (see Table V) observed in the proton-induced reactions on  $^{14}\text{C}$  [26–33, 49–51] supplemented by the behavior of the  $^{14}\text{N}$  neutron cross section to several hundred keV. The  $^{14}\text{C}(p, \gamma)$  reaction has revealed five resonances corresponding to neutron-bound levels of  $^{15}\text{N}$  within the 626-keV window between  $S_n$  and  $S_p$ . The spins and parities ( $J^\pi$ ) of these resonances are also known, some tentatively [42]. A level that possibly has a strong effect on the thermal-neutron scattering of  $^{14}\text{N}$  is the proton resonance at 597 keV (640 keV laboratory energy), which has been found, on the basis of  $\gamma$ -ray angular distribution [26], to have  $J = \frac{3}{2}$  and most probably positive parity. This level lies only  $29 \pm 2$  keV (in the center-of-mass frame) below  $S_n(^{15}\text{N})$ .

If the  $-29$ -keV level is indeed the dominant one governing the scattering length, its putative  $J^\pi = \frac{3}{2}^+$  character leads to the first set of spin-scattering parameters [Eq. 1(a)]. The value of the reduced neutron width for the modification required from a single level to give the  $a_{J=3/2}$  scattering length is deduced from

$$a_J = a_c \{ 1 - \mathcal{R}^\infty - [\gamma_{\lambda(n)}^2 / (E_\lambda - E)] \} \\ \approx a_{\text{pot}} - a_c [\gamma_{\lambda(n)}^2 / (E_\lambda - E)], \quad (2)$$

where  $a_c$  is the channel radius (in  $\mathcal{R}$ -matrix theory) for the entrance channel,  $\mathcal{R}^\infty$  is the more distant-level and background contributions to the  $\mathcal{R}$  function of the single-channel reduced  $\mathcal{R}$ -matrix theory,  $\gamma_{\lambda(n)}^2$  is the reduced neutron width of the level with eigenvalue  $E_\lambda$ ,  $a_{\text{pot}}$  is the potential scattering length from the global optical model, and  $E$  is the neutron energy. Using the modified optical-model parameters of Moldauer [52, 4], the potential scattering length is found to be 4.97 fm; hence, for an assumed channel radius of 3.5 fm, the reduced neutron width of the  $-29$ -keV level is  $\sim 60$  keV (in the laboratory frame of reference).

### B. Resonance parameters

It turns out (see Sec. IV) that the compound-nuclear mechanism plays a substantial role in thermal-neutron capture by  $^{14}\text{N}$ . For its quantitative analysis as much information as possible is needed on nearby resonance levels. More

TABLE I. Energies ( $E_\gamma$ ) and intensities ( $I_\gamma$ ) of  $\gamma$  rays from the  $^{14}\text{N}(n,\gamma)^{15}\text{N}$  reaction.

$E_\gamma$ (keV) <sup>a</sup>	$I_\gamma$ (mb) <sup>b</sup>	Placement <sup>c</sup>	$E_\gamma$ (keV) <sup>a</sup>	$I_\gamma$ (mb) <sup>b</sup>	Placement <sup>c</sup>
131.44 7	0.015 3	$C \rightarrow 10702$	3013.55 10	0.521 17	8313 $\rightarrow$ 5299
383.0 4	0.006 2	$C \rightarrow 10450$	3269.2 4	0.049 9	$C \rightarrow 7564$
583.75 4	0.115 8	9155 $\rightarrow$ 8571	3300.74 13	0.121 9	8571 $\rightarrow$ 5270
608.3 5	0.018 3	9760 $\rightarrow$ 9152	3531.982 20	7.18 9	$C \rightarrow 7301$
767.84 7	0.050 3	$C \rightarrow 10065$	3677.737 17	11.66 13	$C \rightarrow 7155$
770.4 5	0.008 3	9925 $\rightarrow$ 9155	3855.60 7	0.656 21	9155 $\rightarrow$ 5299
831.22 11	0.025 3	7155 $\rightarrow$ 6324	3880.9 9	0.039 13	9152 $\rightarrow$ 5270
908.41 4	0.129 4	$C \rightarrow 9925$	3884.20 9	0.456 18	9155 $\rightarrow$ 5270
1011.68 4	0.110 4	8313 $\rightarrow$ 7301	3923.9 6	0.030 7	9222 $\rightarrow$ 5299
1025.2 3	0.013 2	6324 $\rightarrow$ 5299	4508.731 17	13.42 14	$C \rightarrow 6324$
1053.9 3	0.012 3	6324 $\rightarrow$ 5270	4654.1 11	0.023 5	9925 $\rightarrow$ 5270
1073.02 7	0.071 4	$C \rightarrow 9760$	5269.162 17	23.98 24	5270 $\rightarrow$ 0
1610.79 14	0.059 5	$C \rightarrow 9222$	5297.826 20	17.05 18	5299 $\rightarrow$ 0
1678.293 25	6.39 7	$C \rightarrow 9155$	5533.391 18	15.72 17	$C \rightarrow 5299$
1681.228 50	1.32 3	$C \rightarrow 9152$	5562.059 21	8.58 10	$C \rightarrow 5270$
1783.63 6	0.200 7	$C \rightarrow 9050$	6322.433 16	14.64 18	6324 $\rightarrow$ 0
1853.98 4	0.522 7	9155 $\rightarrow$ 7301	7153.4 4	0.051 6	7155 $\rightarrow$ 0
1884.780 18	15.07 16	7155 $\rightarrow$ 5270	7298.980 32	7.54 10	7301 $\rightarrow$ 0
1988.46 25	0.26 4	8313 $\rightarrow$ 6324	8310.156 39	3.31 7	8313 $\rightarrow$ 0
1999.679 27	3.30 4	9155 $\rightarrow$ 7155	8568.6 4	0.056 5	8571 $\rightarrow$ 0
2002.3 4	0.19 4	7301 $\rightarrow$ 5299	9046.71 17	0.163 9	9050 $\rightarrow$ 0
2030.8 4	0.056 12	7301 $\rightarrow$ 5270	9148.95 9	1.19 5	9152 $\rightarrow$ 0
2247.4 5	0.012 3	8571 $\rightarrow$ 6324	9151.9 7	0.12 3	9155 $\rightarrow$ 0
2261.83 10	0.062 4	$C \rightarrow 8571$	9219.5 11	0.015 6	9222 $\rightarrow$ 0
2293.15 16	0.036 4	7564 $\rightarrow$ 5270	9757.1 5	0.045 5	9760 $\rightarrow$ 0
2520.443 22	4.48 7	$C \rightarrow 8313$	9921.3 3	0.102 8	9925 $\rightarrow$ 0
2726.0 5	0.016 4	9050 $\rightarrow$ 6324	10 061.9 5	0.046 5	10 065 $\rightarrow$ 0
2830.805 36	1.37 3	9155 $\rightarrow$ 6324	10 697.8 17	0.008 4	10 702 $\rightarrow$ 0
2898.4 5	0.018 4	9222 $\rightarrow$ 6324	10 829.110 59	11.5 5	$C \rightarrow 0$

<sup>a</sup>In our notation, 131.44 7  $\equiv$  131.44  $\pm$  0.07, 3013.55 10  $\equiv$  3013.55  $\pm$  0.10, etc.

<sup>b</sup>In our notation, 0.015 3  $\equiv$  0.015  $\pm$  0.003, 0.521 17  $\equiv$  0.521  $\pm$  0.017, etc. Multiply by 1.245 to obtain photons per 100 thermal neutron captures.

<sup>c</sup>See also Table II. The symbol  $C$  denotes the capturing state at 10 833 keV.

precise values of the resonance parameters of the just-bound  $-29$ -keV level, as well as of some other influential levels, can be found by carrying out a multilevel analysis of the neutron total cross-section data up to an energy of about 1 MeV. The relevant levels affecting the  $s$ -wave neutron cross section can be found in Table V. The neutron-resonance parameters listed there are from a preliminary  $\mathcal{R}$ -matrix analysis [53] of several data sets including recent  $^{14}\text{N}+n$  total cross-section data obtained at the Oak Ridge Electron Linear Accelerator (ORELA) [54].

A sharp resonance at 434-keV neutron energy has been found [54] to have  $J = \frac{7}{2}$ , and it is probably a  $d$ -wave resonance. Other important information on the levels governing the neutron cross sections of  $^{14}\text{N}$  can be derived from the  $^{14}\text{C}(p,\gamma)$  and  $^{14}\text{C}(p,n)$  reactions. These reactions provide values of the reduced-width amplitudes for proton emission to the ground state of  $^{14}\text{C}$ , the only significant particle channel other than the neutron channel.

Our independent analysis of the neutron total cross section is based on the reduced  $\mathcal{R}$ -matrix theory with two channels; in this theory, the total cross section is described by

$$\sigma_{n,\text{tot}} = 2\pi\lambda^2 \sum_{J^\pi} g_J (1 - \text{Re} U_{nn}^{J^\pi}) \quad (3)$$

and the neutron-induced proton emission cross section by

$$\sigma_{n,p} = \pi\lambda^2 \sum_{J^\pi} g_J |U_{np}^{J^\pi}|^2, \quad (4)$$

where  $\lambda$  is the de Broglie wave length (divided by  $2\pi$ ),  $g_J$  is the spin-weighting factor, and  $U_{ab}^{J^\pi}$  is the collision matrix element for entrance channel  $a$  and exit channel  $b$  and for total spin and parity  $J^\pi$ ; it is given by

$$U_{ab} = \exp(-i\phi_a) [\mathbf{I} - (\mathcal{S} - \mathcal{B} + i\mathcal{P}\mathcal{R})]^{-1} \times [\mathbf{I} - (\mathcal{S} - \mathcal{B} - i\mathcal{P}\mathcal{R})]_{ab} \exp(-i\phi_b), \quad (5)$$

in which the  $c, d$  element ( $c, d$  also denoting channels) of the reduced  $\mathcal{R}$ -matrix  $\mathcal{R}$  is

TABLE II. Level scheme of  $^{15}\text{N}$  from this work.

$E$ (level) <sup>a</sup> (keV)	$J^\pi$ <sup>b</sup>	Deexciting $\gamma$ rays <sup>c</sup>	$\Sigma I_\gamma$ (in) <sup>a</sup> (mb)	$\Sigma I_\gamma$ (out) <sup>a</sup> (mb)	$\Sigma I_\gamma$ (in-out) <sup>a</sup> (mb)
0.0	$1^-$		79.8 7		79.8 7
5270.164 13	$13^+$	5269.162	24.39 19	23.98 28	0.4 3
5298.824 15	$15^+$	5297.826	17.13 18	17.05 18	0.1 3
6323.858 13	$13^-$	6322.433, 1053.9, 1025.2	15.12 15	14.66 18	0.46 24
7155.089 16	$16^+$	7153.4, 1884.780, 831.22	14.96 14	15.15 16	-0.19 21
7300.885 18	$18^+$	7298.980, 2030.8, 2002.3	7.81 9	7.79 11	0.03 15
7563.53 15	$15^+$	2293.15	0.049 9	0.036 4	0.013 10
8312.635 20	$20^+$	8310.156, 3013.55, 1988.46, 1011.68	4.48 7	4.20 9	0.28 11
8571.20 4	$4^+$	8568.6, 3300.74, 2247.4	0.177 7	0.189 11	-0.012 14
9049.58 6	$6^+$	9046.71, 2726.0	0.200 7	0.179 10	0.021 12
9151.97 5	$5^-$	9148.95, 3880.9	1.34 3	1.23 6	0.11 6
9154.934 18	$18^+$	9151.9, 3884.20, 3855.60, 2830.805, 1999.679, 1853.98, 583.75	6.40 7	6.54 7	-0.14 10
9222.48 14	$14^-$	9219.5, 3923.9, 2898.4	0.059 5	0.063 10	-0.004 12
9760.26 7	$7^-$	9757.1, 608.3	0.071 4	0.063 6	0.008 7
9924.88 5	$5^-$	9921.3, 4654.1, 770.4	0.129 4	0.133 10	-0.004 11
10 065.45 7	$7^+$	10 061.9	0.050 3	0.046 5	0.004 6
10 450.3 <sup>d</sup> 4	$4^-$		0.006 2		0.006 2
10 701.87 <sup>d</sup> 7	$7^-$	10 697.8	0.015 3	0.008 4	0.007 5
10 833.314 <sup>e</sup> 12	$12^+, \frac{3}{2}^+$	10 829.110, 5562.059, 5533.391, 4508.731, 3677.737, 3531.982, 3269.2, 2520.443, 2261.83, 1783.63, 1681.228, 1678.293, 1610.79, 1073.02, 908.41, 767.84, 383.0, 131.44		80.9 6	-80.9 6

<sup>a</sup>In our notation 5270.164 13  $\equiv$  5270.164  $\pm$  0.013, 79.8 7  $\equiv$  79.8  $\pm$  0.7, etc.

<sup>b</sup>Spin and parity assignments for all levels from Ref. [42].

<sup>c</sup>See Table I for intensity values.

<sup>d</sup>Proton unbound.

<sup>e</sup>Capturing state.

$$\mathcal{R}_{cd} = \mathcal{R}_{cd}^\infty + \sum_\lambda \gamma_{\lambda(c)} \gamma_{\lambda(d)} / (E_\lambda - E - i\Gamma_{\lambda, \text{abs}}/2). \quad (6)$$

In Eq. (5),  $\phi_a$  and  $\phi_b$  are the hard-sphere scattering phase shifts for the  $a, b$  channels,  $\mathcal{P}$  and  $\mathcal{S}$  the vector matrices with the penetration and shift factors, respectively, for the neutron and proton channels as elements; these are appropriate to channel radius  $a_c$  and orbital angular momentum  $l$  implied by the  $J^\pi$  of the compound-nuclear state and  $I^\pi$  of the residual nucleus in the appropriate channel, as well as to that the electric charges of the particles in the channel. (For further details, see Lane and Thomas [55].) The quantities in Eqs. (5) and (6) carry an implicit dependence on  $J^\pi$  and, hence, on  $l$ . The reduced  $\mathcal{R}$ -matrix  $\mathcal{R}$  depends only on the levels that carry its implied  $J$  and  $\pi$ . These levels are defined by the internal nuclear Hamiltonian and the boundary conditions  $\mathcal{B}$  imposed at the channel radius. The extra-level parameter  $\Gamma_{\lambda, \text{abs}}$  in Eq. (6) is the ‘‘absorption’’ width into all channels other than the neutron and proton channels. In the  $^{14}\text{N}+n$  case these comprise the radiation channels.

In the analyses described below, the distant level parameters  $\mathcal{R}_{cd}^\infty$  are assumed to be zero for  $c \neq d$  and for the proton channel. Some allowance can be made for inadequate representation of levels near or within the fitted energy range by giving an energy variation to the  $\mathcal{R}_{nn}^\infty$  parameter:

TABLE III. Energies and intensities (photons per 100 neutron captures) of strong  $\gamma$  rays in the reaction  $^{14}\text{N}$  (thermal  $n, \gamma$ ). In our notation, 1678 293 25  $\equiv$  1678 293  $\pm$  25, 7.96 9  $\equiv$  7.96  $\pm$  0.09, etc.

This work Los Alamos		Ref. [24] McMaster <sup>a</sup>	
$E_\gamma$ (eV)	$I_\gamma$ (%)	$E_\gamma$ (eV) <sup>b</sup>	$I_\gamma$ (%)
1678 293 25	7.96 9	1678 174 55	7.23 18
1884 780 18	18.77 20	1884 879 21	18.66 25
1999 679 27	4.11 5	1999 708 86	3.99 9
2520 443 22	5.58 9	2520 418 15	5.79 7
2830 805 36	1.71 4	2830 809 70	1.73 3
3531 982 20	8.94 11	3532 013 13	9.24 9
3677 737 17	14.52 16	3677 772 17	14.89 15
4508 731 17	16.71 17	4508 783 14	16.54 17
5269 162 17	29.86 30	5269 169 12	30.03 20
5297 826 20	21.23 22	5297 817 15	21.31 18
5533 391 18	19.58 21	5533 379 13	19.75 21
5562 059 21	10.68 12	5562 062 17	10.65 12
6322 433 16	18.23 22	6322 337 14	18.67 14
7298 980 32	9.39 12	7298 914 33	9.73 9
8310 156 39	4.12 9	8310 143 29	4.22 5
10 829 110 59	14.3 6	10 829 087 46	13.65 21

<sup>a</sup>This study detected  $\gamma$  rays only in the pair spectrometer mode.

<sup>b</sup>Based on an assumed  $S_n = 10 833.302 \pm 0.012$  keV [34].

TABLE IV. Spectroscopic factors for levels in  $^{15}\text{N}$  from the  $(d,p)$  reaction.

$E$ (level) <sup>a</sup> (keV)	$J^\pi$ <sup>b</sup>	Phillips and Jacobs [45] $E_d=7, 8, \text{ and } 9 \text{ MeV}$ $S(l)$	Amokrane <i>et al.</i> [46] $E_d=3 \text{ MeV}$ $S(l)$	Kretschmer <i>et al.</i> [47] $E_d=10 \text{ MeV}$ $S(l)$	Adopted $S(l)$	Adopted $S(l)$
0.0	$\frac{1}{2}^-$	$1.30 \pm 0.04$ ( $l=1$ )		$1.45 \pm 0.15$ ( $l=1$ )	$1.45 \pm 0.15$ ( $l=1$ )	
5270.164 13	$\frac{3}{2}^+$	$<0.05$ ( $l=2$ )		$<0.22$ ( $l=2$ )		$<0.05$ ( $l=2$ )
5298.824 15	$\frac{1}{2}^+$	$\begin{cases} <0.05 & (l=2) \\ <0.03 & (l=0) \end{cases}$		$<0.03$ ( $l=0$ )		$<0.03$ ( $l=0$ )
6323.858 13	$\frac{3}{2}^-$	$0.10 \pm 0.02$ ( $l=1$ )		$0.11 \pm 0.03$ ( $l=1$ )	$0.11 \pm 0.03$ ( $l=1$ )	
7155.089 16	$\frac{3}{2}^+$	$0.88 \pm 0.03$ ( $l=2$ )		$0.92 \pm 0.07$ ( $l=2$ )		$0.92 \pm 0.07$ ( $l=2$ )
7300.885 18	$\frac{3}{2}^+$	$\begin{cases} 0.07 \pm 0.05 & (l=2) \\ 0.89 \pm 0.04 & (l=0) \end{cases}$		$\begin{cases} 0.07 \pm 0.04 & (l=2) \\ 0.89 \pm 0.05 & (l=0) \end{cases}$		$\begin{cases} 0.07 \pm 0.04 & (l=2) \\ 0.89 \pm 0.05 & (l=0) \end{cases}$
7563.53 15	$\frac{7}{2}^+$	$0.87 \pm 0.01$ ( $l=2$ )				$0.87 \pm 0.01$ ( $l=2$ )
8312.635 20	$\frac{1}{2}^+$	$\begin{cases} <0.09 & (l=2) \\ 1.02 \pm 0.04 & (l=0) \end{cases}$		$\begin{cases} 0.11 \pm 0.05 & (l=2) \\ 0.77 \pm 0.08 & (l=0) \end{cases}$		$\begin{cases} 0.11 \pm 0.05 & (l=2) \\ 0.77 \pm 0.08 & (l=0) \end{cases}$
8571.20 4	$\frac{3}{2}^+$	$\begin{cases} 0.12 \pm 0.03 & (l=2) \\ 0.02 \pm 0.01 & (l=0) \end{cases}$		$\begin{cases} 0.12 \pm 0.05 & (l=2) \\ 0.05 \pm 0.03 & (l=0) \end{cases}$		$\begin{cases} 0.12 \pm 0.05 & (l=2) \\ 0.05 \pm 0.03 & (l=0) \end{cases}$
9049.58 6	$\frac{1}{2}^+$		$0.15$ ( $l=0$ )			$0.15$ ( $l=0$ )
9151.97 5	$\frac{3}{2}^-$		$0.032$ ( $l=1$ )		$0.032$ ( $l=1$ )	
9154.934 18	$\frac{3}{2}^+$		$0.13$ ( $l=2$ )			$0.13$ ( $l=2$ )
9222.48 14	$\frac{1}{2}^-$		$0.045$ ( $l=1$ )		$0.045$ ( $l=1$ )	
9760.26 7	$\frac{5}{2}^-$		$0.021$ ( $l=1$ )		$0.021$ ( $l=1$ )	
9829 3	$\frac{7}{2}^-$					
9924.88 5	$\frac{3}{2}^-$		$\begin{cases} 0.043 & (l=2)^d \\ 0.054 & (l=0)^d \end{cases}$			
10 065.45 7	$\frac{3}{2}^+$	$\begin{cases} 0.48 \pm 0.08 & (l=2) \\ 0.32 \pm 0.08 & (l=0) \end{cases}$	$\begin{cases} 0.64 & (l=2) \\ 0.15 & (l=0) \end{cases}$			$\begin{cases} 0.48 \pm 0.08 & (l=2) \\ 0.32 \pm 0.08 & (l=0) \end{cases}$
10 450.3 <sup>c</sup> 4	$\frac{5}{2}^-$		$0.0082$ ( $l=1$ )		$0.0082$ ( $l=1$ )	
10 533.5 <sup>c</sup> 5	$\frac{3}{2}^+$	$1.06 \pm 0.01$ ( $l=2$ )				$1.06 \pm 0.01$ ( $l=2$ )
10 693.2 <sup>c</sup> 3	$\frac{9}{2}^+$					
10 701.87 <sup>c</sup> 7	$\frac{3}{2}^-$	$\begin{cases} 0.06 \pm 0.03 & (l=2)^d \\ 0.02 \pm 0.03 & (l=0)^d \end{cases}$				
10 804 <sup>c</sup> 2	$\frac{3}{2}^+$	$0.13 \pm 0.01$ ( $l=1$ ) <sup>d</sup>				

<sup>a</sup>In our notation 5270.164 13  $\equiv$  5270.164  $\pm$  0.013, 5298.824 15  $\equiv$  5298.824  $\pm$  0.015, etc.

<sup>b</sup>Spin and parity assignments for all levels from Ref. [42].

<sup>c</sup>Proton unbound.

<sup>d</sup>These  $l$  values are not compatible with the adopted  $J^\pi$ .

$$R_{nn}^\infty = C + D(E - E_{1/2}), \quad (7)$$

where  $E_{1/2}$  is an arbitrarily chosen pivotal energy (usually the midpoint of the range).

The channel radius  $a_c$  and boundary condition  $\mathcal{B}_c$  for a given channel  $c$  are arbitrary parameters in  $\mathcal{R}$ -matrix theory, except for the condition that  $a_c$  should be placed beyond the range of significant nuclear forces. In the case of neutron  $s$  waves, this constraint is not important in practice and, for convenience, a value close to the optical-potential radius is usually chosen. Even for other channels this condition can be overridden to some extent. To obtain realistic energy dependence of the proton-channel penetration factor, a channel radius is adopted that is close to the radius of the Woods-Saxon potential for  $^{14}\text{N}$ . The smooth tail of the real potential well is added to the Coulomb and centrifugal potentials in

order to make numerical calculations of both the penetration and shift factors.

The  $\mathcal{R}$ -matrix eigenvalues  $E_\lambda$  differ from the energies  $E_R$  of isolated resonances:  $E_R = E_\lambda - \Delta_\lambda$ , where the level shift  $\Delta_\lambda = \sum_c (\mathcal{S}_c - \mathcal{B}_c) \gamma_{\lambda(c)}^2$ . The boundary condition  $\mathcal{B}_c$  (the logarithmic derivative of the compound-nuclear wave function projected on the  $c$  channel wave function) imposed at  $a_c$  on the internal eigenfunctions (and their eigenvalues  $E_\lambda$ ) is usually chosen so that the  $E_\lambda$  values coincide as nearly as possible with the resonances in the cross section. In the case of levels open to  $s$ -wave neutrons and with small proton reduced widths, this procedure is achieved with the choice of  $\mathcal{B}_{n(l=0)} = \mathcal{S}_n = 0$ ; for higher orbital angular momenta or for charged-particle channels,  $\mathcal{B}_c$  is chosen to be equal to the shift factor  $\mathcal{S}_c$  at the neutron-separation energy.

With this prescription for  $\mathcal{B}_c$ , the  $\mathcal{R}$ -matrix eigenvalues below the neutron separation energy of  $^{15}\text{N}$  do not coincide

TABLE V. Known resonances in  $^{14}\text{C}+p$  and  $^{14}\text{N}+n$ . Data on the proton resonances are from Refs. [26–33, 49–51]. The neutron resonance parameters are from a preliminary  $\mathcal{R}$ -matrix analysis [53] of all available data including recent total cross-section data [54]. The uncertainty analysis is unavailable at this time, but a rough idea of the uncertainties in the neutron resonance parameters can be obtained from those listed in Ref. [41].

$E_p$ (lab) <sup>a</sup> or $E_n$ (lab) <sup>a</sup> (keV)	$E_x(^{15}\text{N})$ (keV)	$J^\pi$	$E_p$ (c.m.) or $E_n$ (c.m.) (keV)	$E_x(^{15}\text{N})-S_n$ (keV)	$\Gamma_p^b$ (keV)	$\Gamma_n$ (keV)	$[(2J+1)/2]\Gamma_p\Gamma_\gamma/\Gamma$
(a) Resonances in $^{14}\text{C}+p$							
260	10 449.7±0.3	$\frac{5}{2}^-$	242	-384	$(0.08\pm 0.01)\times 10^{-6}$		$(0.29\pm 0.05)$ meV
349	10 533.3±0.5	$\frac{5}{2}^+$	326	-300			$(37\pm 6)$ meV
521	10 693.2±0.3	$\frac{9}{2}^+$	486	-140	$(0.49\pm 0.10)\times 10^{-6}$		$(3.1\pm 0.5)$ meV
530	10 701.9±0.3	$\frac{3}{2}^+$ or $\frac{3}{2}^-$	494	-131	$\sim 0.2$		$(0.84\pm 0.13)$ eV
640 <sup>c</sup>	10 804±2	$\frac{3}{2}^{(+)}$	597	-29	$(0.22\pm 0.10)\times 10^{-3}$		$(0.27\pm 0.04)$ eV
1162	11 291±2	$\frac{1}{2}^-$	1084	458	5.6		
1319	(11 437.6±0.4) <sup>d</sup>	$\frac{1}{2}^+$	1231	605	$6.8\pm 0.5$		
1509	(11 615±4) <sup>e</sup>	$\frac{1}{2}^+$	1408	782	$401\pm 7$		
1668	11 763±3	$\frac{3}{2}^+$	1556	930	0.5		
1788	11 875±3	$(\frac{3}{2})^-$	1668	1042	0.03		
1884	11 965±3	$\frac{1}{2}^-$	1758	1132	0.3		
(b) Resonances in $^{14}\text{N}+n$							
434	11 238	$\frac{7}{2}^+$	405	405	<0.1	2.4	
491	11 291	$\frac{1}{2}^-$	458	458	5.3	1.8	
611	11 403 <sup>e</sup>	$\frac{1}{2}^+, T=\frac{3}{2}$	570	570	250	<5	
634	11 425 <sup>d</sup>	$\frac{1}{2}^+$	591	591	11	26.0	
1000	11 766	$\frac{3}{2}^+$	933	933	0.6	33.7	
1117	11 875	$\frac{5}{2}^-$	1042	1042	<0.2	15.5	
1185	11 938	$\frac{5}{2}^+$	1105	1105	<0.2	1.3	
1210	11 962	$\frac{1}{2}^-$	1129	1129	0.4	11.4	

<sup>a</sup>For an independent evaluation of  $E_p$  (lab) and  $E_n$  (lab) values, see Tables 15.11 and 15.13, respectively, of the latest compilation by Ajzenberg-Selove [41].

<sup>b</sup>The  $\alpha$  widths are negligible compared to the proton widths up to an excitation energy of 13 MeV.

<sup>c</sup>The directly measured  $E_p$  (lab) value of  $635\pm 1$  keV [28,30,33] for this resonance disagrees with  $640\pm 2$  keV deduced from the measured excitation energy of  $10\,804\pm 2$  keV [32] given in the next column. The conclusions of this paper are relatively unaffected by this change.

<sup>d</sup>The 11 438-keV level seen in  $^{14}\text{C}+p$  and the 11 425-keV level seen in  $^{14}\text{N}+n$  are probably the same. This is a broad level.

<sup>e</sup>The 11 615-keV level seen in  $^{14}\text{C}+p$  and the 11 403-keV level seen in  $^{14}\text{N}+n$  are probably the same. This is a very broad level.

with the neutron-bound states  $E'_\lambda$  (seen in the  $^{12}\text{C}+p$  reaction) that influence the low-energy neutron cross section, the latter having a natural boundary condition in the neutron channel equivalent to  $\mathcal{B}_n = -\kappa(E'_\lambda)a$ , giving rise to a level-shift contribution of  $-\kappa(E'_\lambda)a\gamma_{\lambda(n)}^2$ . Here,  $\kappa(E'_\lambda) = \sqrt{2M|E'_\lambda|/\hbar^2}$ ,  $M$  being the reduced mass of neutron+target. For levels with large reduced proton widths, even larger contributions to the level shifts can occur from the energy dependence of the proton shift factor.

The reduced neutron widths of many of the negative-energy ( $s$ -wave)  $\mathcal{R}$ -matrix levels were estimated from the spectroscopic factors of the corresponding bound states (when available); this was done for most of the states up to an excitation energy of 9.5 MeV in  $^{15}\text{N}$ . The reduced widths of schematic single-particle  $\mathcal{R}$ -matrix levels were first calculated as a function of binding energy for a potential of Woods-Saxon shape with parameters appropriate for  $^{14}\text{N}$ , the binding energy being varied by changing the potential depth. The single-particle reduced width thus calculated at

the binding energy of the appropriate  $\mathcal{R}$ -matrix level was then multiplied by the spectroscopic factor of the corresponding bound state. Reduced widths, level shifts, and  $\mathcal{R}$ -matrix binding energies were calculated in an iterative process starting from the energies of the bound states  $E'_\lambda$ . In the discussion below, the proton resonances below  $S_n(^{15}\text{N})$  (the ‘‘bound levels’’) are referred to by their energies  $E'_\lambda$  or  $(E'_\lambda - S_n)$  in the center-of-mass system.

The spins and parities of most of the neutron-bound  $J^\pi = \frac{1}{2}^+, \frac{3}{2}^+$  levels seem to be well determined. Two of the least certain assignments, however, belong to levels that concern us most. One of these at -29 keV has already been mentioned. The other is a resonance at 494 keV observed in the  $^{14}\text{C}(p, \gamma)$  reaction. This level is bound by 131 keV against neutron emission. The spin of this level is  $\frac{3}{2}$ , but conflicting attributions have been made for its parity. Hebbard and Dunbar [28] assign positive parity from proton elastic scattering measurements and compilations prior to 1976 (see footnote 1) show this assignment, but later compilations [42] show

negative parity based on the unpublished work of Beukens [32]. The partial widths of the  $-29$ -keV level account only for  $\sim 10\%$  of the (thermal  $n,p$ ) cross section. The  $131$ -keV level has a large proton width ( $\sim 200$  eV [42]), and a positive-parity assignment would account for the major portion of the (thermal  $n,p$ ) cross section.

In our  $\mathcal{R}$ -matrix analysis (in which the level at  $-131$ -keV is included as a  $\frac{3}{2}^+$  state) all known  $J^\pi = \frac{1}{2}^+$  and  $J^\pi = \frac{3}{2}^+$  bound states were included explicitly. The reduced neutron widths of the states below  $9.5$ -MeV excitation energy were held at the fixed values determined using the ( $d,p$ ) spectroscopic factors. Qualitative information on the reduced neutron widths of the higher-lying states can be found in the literature on the ( $d,p$ ) reaction. Phillips and Jacob [45] find stripping cross sections to the  $10\ 702$ - and  $10\ 804$ -keV states that are only a small fraction of that to the  $7301$ -keV state. In more recent work, Piskoř and Schäferlingová [56] make no mention of states between  $10.07$  and  $11.23$  MeV, again indicating weak stripping cross sections and, therefore, small reduced neutron widths. By contrast, the  $-767$ -keV level (excitation energy  $10\ 066$  keV) shows up as quite a strong state with a cross section perhaps about half that of the  $7301$ -keV state [45,56]. In Ref. [45] its stripping pattern is described as a mixture of  $l=2$  and  $l=0$ , with an attempt made at assigning the relative weight of the spectroscopic factors.

Information on the reduced proton widths of the two weakly (neutron-)bound levels and some of the unbound levels can be obtained from the  $^{14}\text{C}+p$  reactions. The proton widths  $\Gamma_p$  recommended in Ref. [42] for the  $-29$ - and  $-131$ -keV levels are listed in Table V. Measurements by Bartholomew *et al.* [26] of the ( $p,n$ ) and ( $p,\gamma$ ) yields over the two nearly overlapping and strongly interfering  $J^\pi = \frac{1}{2}^+$  resonances in the  $1.1$ – $1.5$  MeV proton energy region ( $0.5$ – $0.9$  MeV neutron energy) have been analyzed by Ferguson and Gove [27] to yield proton and neutron reduced width amplitudes. Because of the large value of its reduced proton width, the  $-131$ -keV level makes an important contribution to the (thermal  $n,p$ ) cross section of  $^{14}\text{N}$ . This contribution can be enhanced by the sign relationships of the reduced width amplitudes of the  $J^\pi = \frac{1}{2}^+$  levels that give constructive interference between their contributions to that cross section. Therefore, the measured (thermal  $n,p$ ) cross section ( $\sigma_{np} = 1.83 \pm 0.03$  b [57]) can be used to constrain the possible values of the reduced neutron width of the  $-131$ -keV level.

The remaining  $\mathcal{R}$ -matrix parameters, including the important reduced neutron width of the  $-29$ -keV level, were deduced by least-squares analysis of the neutron total cross section (data of Harvey and co-workers [54] averaged in energy bins of varying widths), the thermal-neutron-scattering lengths, and the (thermal  $n,p$ ) cross section, the ( $n,p$ ) cross-section data of Morgan [58] up to  $1$  MeV neutron energy, and some ( $n,p$ ) cross-section data [59,60] at lower neutron energies. After trial adjustment of some of the more distant levels, such as the  $J^\pi = \frac{3}{2}^+$  resonance at  $1$  MeV, a best fit to the reduced neutron width amplitudes of the levels at  $-29$  and  $-131$  keV and to the  $\mathcal{R}_{3/2}^\infty$  parameter gave us the fit shown in Fig. 5 with the parameters listed in Table VI. In spite of the small proton reduced width of the  $-29$ -keV level (denoted by  $\lambda$ ), the interference of this level with the

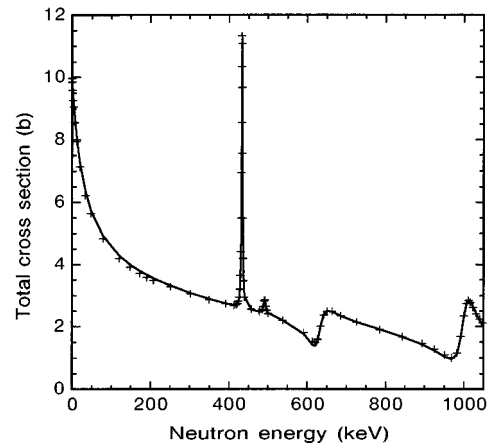


FIG. 5. Total neutron cross section of  $^{14}\text{N}$  fitted with the parameters of Table VI.

contribution of the  $-131$ -keV level (denoted by  $\mu$ ) has an appreciable effect on the (thermal  $n,p$ ) cross section. Thus, the assumption about the relative signs of the reduced proton width amplitudes of these two levels has a marked effect on the resulting value of the reduced neutron width of the lower level. Acceptable fits can be found for a range of values for the neutron widths of these two levels, the correlation being (units in keV)

$$\gamma_{\mu(n)}^2 = (509 - 9.6\gamma_{\lambda(n)}^2). \quad (8)$$

Uncertainties in the reduced width amplitudes of the major neutron resonances up to  $1$  MeV are  $\sim 1\%$ .

In the above analysis, the assumption has been made that the  $-131$ -keV level has  $J^\pi = \frac{3}{2}^+$ . The positive-parity assignment was made by Hebbard and Dunbar [28], who observed an anomaly in the  $^{14}\text{C}(p,p)$  elastic scattering which could be explained if this resonance were a  $d$  wave. However, according to Beukens [32], the positive-parity assignment should be ruled out because it would lead to a prohibitively large  $M2$  strength of  $15 \pm 4$  Weisskopf units for the transition to the  $9222$ -keV,  $\frac{1}{2}^-$  level. We believe strongly that the  $\frac{3}{2}^+$  assignment is correct because the  $-29$ -keV level on its own falls short of explaining the low-energy  $^{14}\text{N}(n,p)$  cross section by at least one order of magnitude. Nevertheless, in the following analysis of the neutron-capture  $\gamma$ -ray data, we do consider the possibility that the  $-131$ -keV level has negative parity and does not contribute to the  $s$ -wave neutron cross sections. We note here that to fit the total cross-section data in this case, the reduced neutron width amplitude of the  $-29$ -keV level becomes  $235$  eV $^{1/2}$ .

#### IV. PRIMARY $E1$ TRANSITIONS

Direct (thermal  $n,\gamma$ ) can be described in simple terms as the transition from the orbit of a neutron being scattered by a smooth potential field to the single-particle component of the bound final state. The important fact that makes this process rather precisely calculable is the location of the major part of the integrand of the radial matrix element beyond the nuclear potential radius (“channel capture” [1]). Here the wave functions involved can be rather accurately constructed, usu-

TABLE VI. Resonance parameters for the total neutron cross section and spin-state neutron scattering lengths of  $^{14}\text{N}$  over the neutron energy range 0–1 MeV. The channel radius  $a_c=4.0$  fm. The “pivot” energy  $E_{1/2}$  for Eq. (7) and for evaluation of boundary conditions is zero. The absorption width  $\Gamma_{\text{abs}}$  is assumed to be 0.5 eV. Eigenvalues  $E_\lambda$  are given in the laboratory frame.

$J^\pi$	$C$	$D$ (eV $^{-1}$ )	$E_\lambda$ (keV)	$\gamma_{\lambda(n)}$ (eV $^{1/2}$ )	$\gamma_{\lambda(p)}$ (eV $^{1/2}$ )	$\Gamma_{\lambda(n)}$ (keV)	$\Gamma_{\lambda(n)}^0$ (eV)	$\Gamma_{\lambda(p)}$ (keV)
$\frac{1}{2}^+$	-0.57	$2 \times 10^{-7}$	-5933	47 <sup>a</sup>			3.6	
			-3210	394 <sup>b</sup>			254	
			-1906	50 <sup>a</sup>			47	
			635	154	-59	30.8	39	6.23
			890	50 <sup>c</sup>	408 <sup>c</sup>	3.87	4.1	400
$\frac{3}{2}^+$	0.024	-0.000	-4301	543 <sup>b</sup>			483	
			-2462	167 <sup>b</sup>			46	
			-830	467 <sup>d</sup>			358	
			-175	122	735 <sup>e</sup>		24	0.17
			-42	227	12		84.5	$1.2 \times 10^{-4}$
			998	163	-115	43.5	43.5	34.9
$\frac{1}{2}^-$	~0.000	~0.000	501	82	158	0.98		6.56
			1116	185	70	12.7		4.4
			470	577	108	1.86		0.13

<sup>a</sup>Assumed value; negligible or small  $l=0$  ( $d,p$ ) strength (see Table IV).

<sup>b</sup>From ( $d,p$ ) spectroscopic factor (see Table IV).

<sup>c</sup>Width parameter from Table V.

<sup>d</sup>Assumed value from qualitative indications of the ( $d,p$ ) strength [45].

<sup>e</sup>From ( $p,\gamma$ ) reactions [33].

ally from a knowledge of the neutron-scattering length, the binding energy, and the single-particle spectroscopic factor of the final state. The wave functions can be refined by calculating them within the framework of an optical model [1,2]. A by-product of this calculation arises from the imaginary part of the optical potential, yielding a cross-section component proportional to the valence-radiation strength function. Valence radiative capture is the resonance analog of the off-resonance direct capture [61,62].

The formal theory of direct capture is described in Refs. [1,2,62,63], and methods for calculating direct-capture cross sections from the optical model to compare with experimental data are given in Refs. [2,4,6]. In Refs. [4] and [6] two useful practical methods were developed. In the first method, the parameters of the global optical potential are modified, within reasonable physical limits, to reproduce the actual slow-neutron-scattering length of the target nucleus. For the final state, the well depth of the real component of the optical potential is modified so that the single-particle final state has its eigenvalue equal to the binding energy of the actual final state of the compound nucleus. The radiative transition strength is computed from the radial matrix element formed between the wave functions of scattering and bound state of these two potentials and multiplied by the spectroscopic factor of the actual final state. This method is known as the specialized ( $S$ ) optical-potential method.

In the second method, the initial-state-scattering wave function is calculated without modifying the global optical-potential parameters, except that the real potential for the final state eigenfunction is still varied to give the required binding energy. The discrepancy between the computed neutron-scattering length (the potential-scattering length) and the experimental value is attributed to the influence of one or

more local resonance levels (bound or unbound). A valence radiative component proportional to this difference is added to the potential-capture amplitude calculated from the global optical potential. The valence radiation width is derived from an imaginary term in the dipole radial matrix element that arises from the presence of the imaginary component of the optical potential. The direct-capture cross section thus calculated is known as the global+valence ( $G+V$ ) result. Our experience with the two methods is that their results normally agree to within a few percent.

For the  $J^\pi = \frac{3}{2}^+$  scattering state of  $^{14}\text{N}+n$ , it turns out that the contribution from the valence amplitude is much greater in magnitude than that from potential capture. Because of the greater modeling uncertainties in extracting the valence component from the optical-model calculation, the ( $S$ ) method for calculating the direct-capture component has been relied upon in this work. The parameter chosen to vary to reproduce the scattering lengths is the real potential depth. For this type of variation to succeed in reproducing the  $J = \frac{3}{2}$  scattering length without altering the global potential radius or surface diffuseness parameter, the imaginary component of the optical potential was set to zero. This procedure should realistically represent the scattering in the region beyond the potential radius where the contribution to the radial component of the  $E1$  matrix element is by far the major one. For these ( $S$ ) calculations the modified Moldauer parameters [2,52] are used for the global optical potential. The results of our calculations for the  $E1$  primary transitions in  $^{15}\text{N}$  are compared with measurements in Table VII.

In view of the previous success of the direct-capture theory in explaining  $E1$  capture cross sections in the  $0p$  shell [4,13], not to mention the general success of the theory

TABLE VII. Direct-capture cross sections for primary  $E1$  transitions in the  $^{14}\text{N}(n, \gamma)$  reaction. Calculations use the experimental scattering lengths  $a_{J=1/2}=6.3$  fm and  $a_{J=3/2}=10.0$  fm. The calculated neutron strength function  $\bar{\Gamma}_n^0/D$  is  $2.003 \times 10^{-4}$ . Columns 1, 2, 3, and 4 give the energy,  $J^\pi$  value, transferred  $j$  value, and the  $l=1$  ( $d, p$ ) spectroscopic factor multiplied by  $(2J+1)$  for the final state, respectively. Column 5 is the primary transition energy. Column 6 is the average valency capture width and column 7 the potential capture cross section, both calculated using the specialized optical model. The entries in column 6 do not include the spin-coupling factor and the spectroscopic factor; those in column 7 do. Column 8 is the calculated cross section using the specialized optical-model ( $S$ ) procedure. The measured cross sections are given in column 9. Finally, column 10 gives the hypothesized compound-nuclear contributions deduced from the differences between column 8 and column 9 via Eq. (9); they are presented as two alternative values separated by a solidus.

$E_f$ (keV)	$J^\pi$	$j$	$(d, p)$ $(2J+1)S$	$E_\gamma$ (keV)	$\Gamma_{\gamma, \text{val}}/DE_\gamma^3$ ( $10^{-7}$ MeV $^{-3}$ )	$\sigma_{\text{pot}, \gamma}$ (mb)	$\sigma_{\text{dir}, \gamma}(S)$ (mb)	$\sigma_{\text{exp}, \gamma}$ (mb)	$\sigma_{\text{CN}, \gamma}$ (mb)
0	$\frac{1}{2}^-$	$\frac{1}{2}$	2.90	10 829	0.181	0.16	280.4	11.5 5	178/405
6324	$\frac{3}{2}^-$	$\frac{3}{2}$	0.44	4509	0.978	0.74	5.47 <sup>a</sup> 3.68 <sup>b</sup>	14.64 18	2.2/38 3.6/33
9152	$\frac{3}{2}^-$	$\frac{1}{2}$ $\frac{3}{2}$	0.13	1681	0.770 2.400	0.52 0.44	9.15 0.14 <sup>a</sup>	1.32 3	0.6/47 0.6/2.3
9222	$\frac{1}{2}^-$	$\frac{3}{2}$	0.09	1611	2.130 2.519	0.43 0.31	0.14 <sup>b</sup> 0.14 <sup>a</sup>	0.059 5	0.02/0.4
9760	$\frac{5}{2}^-$	$\frac{3}{2}$	0.13	1073	2.238 3.808	0.30 0.11	0.14 <sup>b</sup> 0.06 <sup>a</sup>	0.071 4	0.00/0.3
9925	$\frac{3}{2}^-$	$\frac{3}{2}$		908	4.094	$9.2 \times S$	$3.37 \times S^b$	0.129 4	
10 450	$\frac{3}{2}^-$	$\frac{3}{2}$	0.05	383	9.775	0.006	0.013 <sup>b</sup>	0.006 2	0.00/0.04
10 702	$\frac{3}{2}^-$	$\frac{3}{2}$		131	28.16	$1.8 \times S$	$1.30 \times S^b$	0.015 3	

<sup>a</sup>Assumed  $0p_{3/2}$  final-state single-particle character.

<sup>b</sup>Assumed  $1p_{3/2}$  final-state single-particle character.

when applied to ( $A < 50$ ) nuclides [1,6], it is surprising to see the apparent failure of the theory [compare the  $\sigma_{\text{dir}, \gamma}(S)$  and  $\sigma_{\text{exp}, \gamma}$  columns of Table VII] in the current case. For the transition to the ground state, which has an almost pure  $0p_{1/2}$  configuration, the measured cross section is only about  $\frac{1}{25}$  of the theoretical cross section, while for the transition to the 6324-keV state, the measured cross section is 1.5 to 4 times greater than theory suggests. If the influence of compound-nuclear components in the transitions is responsible for these discrepancies, the relation

$$\sigma_{\text{CN}, \gamma} = [\sigma_{\text{dir}, \gamma}^{1/2} \pm \sigma_{\text{exp}, \gamma}^{1/2}]^2 \quad (9)$$

can be used to infer that the compound-nuclear component has to be of similar magnitude to the direct component. It is noted also that the totals of both the calculated direct-capture cross sections and the apparent compound-nuclear capture cross sections are much greater than the experimental value of the total capture cross section. Further analysis of the role of compound-nuclear capture can be made using the estimated properties of the bound levels from Sec. III B. This analysis is postponed to Sec. VI following our analysis of the  $M1$  transitions in the next section which yields more information on bound-level properties.

## V. PRIMARY $M1$ TRANSITIONS

The cross sections of ten primary  $M1$  transitions (compared to eight primary  $E1$  transitions) have been measured in the  $^{14}\text{N}$  (thermal  $n, \gamma$ ) reaction. The average cross section of the  $M1$  transitions is actually greater than that of the  $E1$  by

a factor of 2. This is the strongest example to date of the nonconformance of slow- and resonance-neutron capture with the multipolarity rules of Blatt and Weisskopf [64].

With the expectation, and observation in ( $d, p$ ) reactions, that the  $1s_{1/2}$  single-particle neutron state is bound by a few MeV in  $^{15}\text{N}$ , it is tempting to test the magnetic-dipole version of direct-capture theory against the data. Direct  $M1$  neutron capture can only be a spin-flip process with no orbital angular momentum change involved. It depends for its existence on the scattering and final states being controlled by rather different potential fields.

The calculation of the direct  $M1$  capture cross section is identical to the procedure for  $E1$  in either the ( $S$ ) or ( $G+V$ ) methods (see Sec. IV), except that the  $E1$  operator  $rY_{1\mathcal{M}}$  (see Eq. (13) of Ref. [8]) is replaced by the  $M1$  operator. The simple form for this operator for a neutron (magnetic moment  $\mu_n$  in nuclear magnetons) impinging on the potential field provided by a target nucleus with magnetic moment  $\mu_I$  is

$$\mathcal{H}'_{M1, \mathcal{M}} = \frac{e\hbar}{2mc} \left[ \frac{3}{4\pi} \right]^{1/2} \left[ \frac{\mu_I I_{\mathcal{M}}}{I} + \frac{\mu_n \sigma_{n, \mathcal{M}}}{\sigma} \right]. \quad (10)$$

Here  $e$  is the proton charge,  $m$  the nucleon mass,  $c$  the velocity of light,  $I$  the target-nucleus spin operator,  $\mathcal{M}$  the polarization quantum number, and  $\sigma$  the Pauli spin operator for the neutron. From this expression the reduced matrix element for the spin factor can be computed, while the radial matrix element is simply the integral of the product of the initial state radial wave function  $X_\lambda$  and the final state radial wave function  $\Phi_\mu$  projected on the single-particle channel.

TABLE VIII. Direct-capture cross sections for primary  $M1$  transitions in the  $^{14}\text{N}(n, \gamma)$  reaction. Columns 1, 2, 3, and 4 give the energy,  $J^\pi$  value, transferred  $l$  value, and the  $(d, p)$  spectroscopic factor multiplied by  $(2J+1)$  for the final state, respectively. Column 5 is the primary transition energy. Column 6 is the average valency capture width and column 7 the potential capture cross section, both calculated using the specialized optical model. The entries in column 6 do not include the spin-coupling factor and the spectroscopic factor; those in column 7 do. Column 8 is the calculated cross section using the specialized optical-model ( $S$ ) procedure. The measured cross sections are given in column 9.

$E_f$ (keV)	$J^\pi$	$l$	$(d, p)$ $(2J+1)S$ ( $l$ )	$E_\gamma$ (keV)	$\Gamma_{\gamma, \text{val}}/DE_\gamma^3$ ( $10^{-9} \text{ MeV}^{-3}$ )	$\sigma_{\text{pot}, \gamma}$ (mb)	$\sigma_{\text{dir}, \gamma} (S)$ (mb)	$\sigma_{\text{exp}, \gamma}$ (mb)
5270	$\frac{5}{2}^+$	2	<0.3 (2)	5562	0.141			8.58 10
5299	$\frac{1}{2}^+$	0+2	<0.06 (0)	5533	0.143	$<20 \times 10^{-6}$	<0.38	15.72 17
7155	$\frac{5}{2}^+$	2	5.5 (2)	3678	0.181			11.66 13
7300	$\frac{3}{2}^+$	0+2	3.6 (0)	3532	0.186	0.11	7.31	7.18 9
8312	$\frac{1}{2}^+$	0+2	1.54 (0)	2520	0.226	0.10	1.35	4.48 7
8571	$\frac{3}{2}^+$	0+2	0.2 (0)	2262	0.241	0.009	0.108	0.062 4
9050	$\frac{1}{2}^+$	0	0.30 (0)	1784	0.276	0.020	0.081	0.200 7
9155	$\frac{5}{2}^+$	2	0.78 (2)	1678	0.286			6.39 7
10 066	$\frac{3}{2}^+$	0+2	1.3 (0)	768	0.439	0.032	0.027	0.050 3
10 533	$\frac{5}{2}^+$	2	6.4 (2)	300				<0.01

In the current calculations, the modified Moldauer optical-model parameters are used. For the initial state, the well depth of  $-46$  MeV is used in the  $(G+V)$  method, but it is adjusted to reproduce the scattering length in the  $(S)$  method; in the latter, the imaginary component of the optical potential is set to zero. For the final state, the well depth is adjusted to reproduce the binding energy of the state. The magnetic moment for  $^{14}\text{N}$  is  $0.4038$  nuclear magnetons [42].

The calculated direct-capture cross sections are shown in Table VIII and compared therein with the data. Three of the strongest measured transitions are to  $J^\pi = \frac{5}{2}^+$  final states at 5270, 7155, and 9155 keV which can only be formed from single-particle states with  $l=2$  and, therefore, have zero direct cross sections. For the same reason, the direct-capture cross section of the transition to the 10 533-keV,  $\frac{5}{2}^+$  state is also zero. The strongest cross section of all primary  $M1$  transitions is for the 5533-keV transition to the 5299-keV,  $\frac{1}{2}^+$  state, but this state is reported as having no clear stripping pattern [45] and, in any case, it has a very small  $(d, p)$  spectroscopic factor. Consequently, the direct-capture cross section of the 5533-keV transition must be very small.

For all five of the remaining transitions to the states at 7301, 8313, 8571, 9050, and 10 065 keV, the direct-capture cross sections can be calculated; there is semiquantitative agreement (compare the last two columns of Table VII) with the experimental values. It can be concluded that direct capture may be playing a significant role in these transitions but not a dominant one. The evidence of the strongest transitions is that the  $M1$  giant resonance, involving a cooperative spin flip between the  $0d_{3/2}$  and  $0d_{5/2}$  subshells at an energy of 2 to 5 MeV, could be playing a major role.

That the  $M1$  transitions from (thermal  $n, \gamma$ ) are governed more by the  $-29$ -keV level (the 640-keV proton resonance) rather than by a dominant admixture of direct capture is further demonstrated by using information from the  $^{14}\text{C}(p, \gamma)$  reaction. From the resonance parameters that govern the  $^{14}\text{N}$  neutron cross section (see Table V), it is seen that the  $-29$ -keV level will dominate the resonance contribution to

the thermal-capture cross section; no other level will contribute more than a few percent, assuming similar radiation widths, apart from possibly the  $-131$ -keV level. If the  $-131$ -keV level has positive parity as assumed in the  $\mathcal{R}$ -matrix analysis of Sec. III B, its  $J = \frac{3}{2}$  character allows an amplified effect through interference with the capture amplitude from the  $-29$ -keV level.

To evaluate the contribution from the  $-29$ -keV level, the data used are (i)  $\Gamma_{\lambda(p)}\Gamma_{\lambda(\gamma)}/\Gamma_\lambda = 135 \pm 20$  meV [33], (ii)  $\Gamma_{\lambda(\gamma)}/\Gamma_\lambda = 0.55^{+0.25}_{-0.15}$  [65], and (iii) the primary capture  $\gamma$ -ray spectrum [33]. The combination of (i) and (ii) gives  $\Gamma_{\lambda(\gamma)} = 300^{+470}_{-110}$  meV for the total radiation width of this resonance, the bulk of the uncertainty coming from the  $\Gamma_{\lambda(\gamma)}/\Gamma_\lambda$  measurement. Using the spectral information, the partial radiation widths for the primary  $M1$  transitions can be determined.

The nondirect transitions to the three  $J^\pi = \frac{5}{2}^+$  final states are examined first, neglecting the possible influence of the  $-131$ -keV level. From the thermal-neutron cross sections (assuming them to arise from only the spin  $\frac{3}{2}$  initial state), the partial radiation widths (the compound-nuclear radiation widths of the  $-29$ -keV level) for these transitions can be calculated as a function of this level's reduced neutron width using the formula

$$\sigma_{\gamma(\text{CN}), \lambda} = \pi \lambda^2 g_\lambda \Gamma_{\lambda n}(\text{th}) \Gamma_{\lambda \gamma(\text{CN}), i} / E_\lambda^2 \quad (11)$$

for the cross section of the  $i$ th transition, where  $\Gamma_{\lambda n}(\text{th}) = 2ka \gamma_{\lambda(n)}^2$  is the neutron width of the level  $\lambda$  at thermal-neutron energy. These partial widths can be divided by the respective spectral abundances in the  $-29$ -keV  $^{14}\text{C}(p, \gamma)$  resonance to determine three values of the total radiation width. Within the likely range of the reduced neutron width, they are in agreement with each other (within two or three standard deviations), but are a little higher than the (broad) estimate of the total radiation width from the  $(p, \gamma)$  data discussed above. From this spectral analysis, it is concluded

that the likely value of the total radiation width ranges from about 1000 meV (if the reduced neutron width is  $\sim 49$  keV) to about 900 meV (if the reduced width is  $\sim 53$  keV).

The transitions to the  $J^\pi = \frac{3}{2}^+$  and  $J^\pi = \frac{1}{2}^+$  final states are examined next, ignoring at first the direct component. With the same treatment as above, results are obtained that are in substantial agreement among the three transitions for which all the relevant data are available, but the total radiation widths lie about 25% lower than those from the transitions to the  $J^\pi = \frac{5}{2}^+$  levels.

Inclusion of the  $-131$ -keV level complicates the analysis. Fortunately, the total radiation width of this level is known accurately from the  $^{14}\text{C}(p, \gamma)$  work; it is  $\Gamma_{\gamma(\text{tot})} = 420 \pm 65$  meV [33]. When combined with the spectral abundance data, the partial radiation widths can be determined. With the value of the reduced neutron width taken from Eq. (7), it is possible to make an estimate of the contribution of the  $-131$ -keV level to the (thermal  $n, \gamma$ ) cross-section amplitudes. Using

$$\sigma_{\lambda(\gamma, i)} = [\sigma_{\mu(\gamma, i)}^{1/2} \pm \sigma_{\text{exp}(\gamma, i)}^{1/2}]^2, \quad (12)$$

the contribution from the  $-29$ -keV level can be extracted, which is then analyzed as before. The major effect is on the  $5562$ -keV transition to the  $5270$ -keV final state because this transition is very strong in the  $-131$ -keV proton resonance spectrum. Two branches are now found for  $\Gamma_{\gamma(\text{tot})}$  corresponding to the interference implied in Eq. (11). One branch runs from  $\sim 400$  meV for  $\gamma_{\lambda(n)}^2 = 49$  keV to  $\sim 800$  meV for  $\gamma_{\lambda(n)}^2 = 53$  keV; the other from  $\sim 1800$  to  $\sim 1000$  meV over the same range. The splitting between the branches found for the other two transitions is not nearly so great; in fact, it is much less than the uncertainty caused by the experimental uncertainties in the spectral factor  $f_{\gamma, i}$ . The branches that are in agreement for the three transitions are shown in Fig. 6(a).

The transitions to the  $\frac{1}{2}^+$  and  $\frac{3}{2}^+$  final states are not strongly affected by the  $-131$ -keV level, so further consideration of these transitions is deferred to the next section.

## VI. DIRECT AND RESONANCE INTERPLAY

In a more elaborate way, the primary  $E1$  transitions in the  $^{14}\text{N}$  (thermal  $n, \gamma$ ) can be compared with those measured in the  $^{14}\text{C}(p, \gamma)$  work. The strengths of the three  $E1$  transitions to the  $0.0$ -,  $6324$ -, and  $9152$ -keV levels from the  $-29$ -keV proton resonance are [33]  $(44 \pm 4)$ ,  $(6.8 \pm 0.7)$ , and  $(2.9 \pm 0.4)$  %, respectively. These values are to be compared, respectively, with  $(14.3 \pm 0.7)$ ,  $(16.7 \pm 0.3)$ , and  $(1.6 \pm 0.1)$  % from the current  $^{14}\text{N}$  (thermal  $n, \gamma$ ) work. The pattern of partial radiation widths that emerges from the (resonance  $p, \gamma$ ), after assuming a reasonable value of the total radiation width, is quite different from that needed to explain the (thermal  $n, \gamma$ ) spectrum. For example, if a total radiation width of  $600$  meV and a reduced neutron width of  $50$  keV are assumed, the resonance contribution to the partial capture cross sections for these three  $E1$  transitions are  $37$ ,  $5.7$ , and  $2.4$  mb compared, respectively, to the measured values (see Table I) of  $11.5$ ,  $13.4$ , and  $1.3$  mb. Reference to the compound-nuclear cross-section entries in Table VII shows

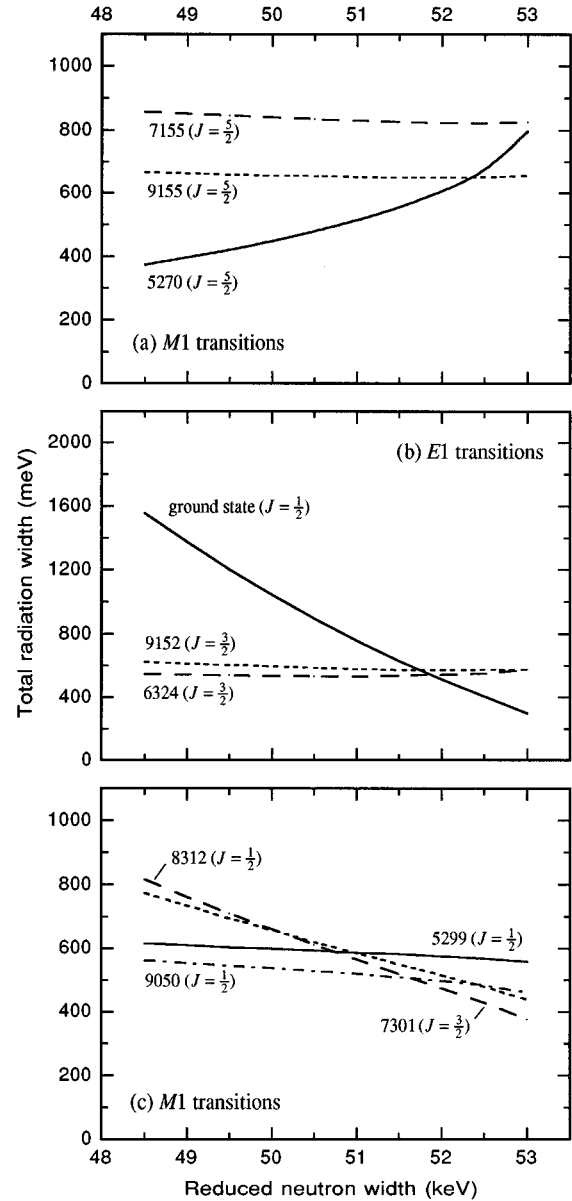


FIG. 6. Total radiation width of the  $-29$ -keV level deduced from (a)  $M1$  transitions to  $J^\pi = \frac{5}{2}^+$  final states, (b)  $E1$  transitions to  $J^\pi = \frac{1}{2}^+$  and  $J^\pi = \frac{3}{2}^+$  final states, and (c)  $M1$  transitions to  $J^\pi = \frac{1}{2}^+$  and  $J^\pi = \frac{3}{2}^+$  final states. Allowance has been made for direct capture in the  $(n, \gamma)$  reaction.

that the latter values are also quite unlike the resonance contribution. A likely explanation for these strong differences is that there is a substantial component of neutron valence amplitude in the transitions from the bound level, and this component interferes with the compound-nuclear amplitude to give the distinctive resonance spectrum that is observed; this spectrum differs from the (thermal  $n, \gamma$ ) spectrum because of the interference in  $(n, \gamma)$  with the potential-capture amplitude. A quantitative analysis of this hypothesis now follows.

The procedure used is the following. First, it is assumed that the compound-nuclear process contributes only to the  $J = \frac{3}{2}$  component of the cross section, the local levels that can influence the capture cross section being only of this spin. The calculated value of the  $J = \frac{1}{2}$  direct-capture cross section is then deducted from the experimental value of the capture

cross section; this is denoted as the  $J=\frac{3}{2}$  experimental cross section. Next, the compound-nuclear cross section  $\sigma_{\gamma(\text{CN})i}$  for each transition is deduced from the difference between the  $J=\frac{3}{2}$  direct and experimental capture cross-section amplitudes [see Eq. (9)]. The two possible values for this are very close to those that have already been given in Table VII, the  $J=\frac{1}{2}$  direct-capture cross section being very small. Then a value of the reduced neutron width of the  $-29$ -keV level is selected from the range that gives a reasonable fit to the total neutron cross section (see Sec. III). This selection also implies [from Eq. (7)] a value for the reduced width of the  $-131$ -keV level. Hence, it is possible to calculate (see below) the value of the valence radiation width for this state as well as for the  $-29$ -keV state. After using

$$\Gamma_{\mu,\gamma(\text{CN})i}^{1/2} = \Gamma_{\mu,\gamma i}^{1/2} \pm \Gamma_{\mu,\gamma(\text{val})i}^{1/2}, \quad (13)$$

two possible values can be calculated for the contribution to the compound-nuclear capture cross section resulting from the  $-131$ -keV level acting alone. With this information, four possible values can be extracted for the compound-nuclear capture cross section resulting from the  $-29$ -keV level using

$$\sigma_{\lambda,\gamma(\text{CN})i} = [\sigma_{\gamma(\text{CN})i}^{1/2} \pm \sigma_{\mu,\gamma(\text{CN})i}^{1/2}]^2. \quad (14)$$

Hence, the compound-nuclear radiation width can be calculated using Eq. (11). Combining the radiation width amplitudes for the valence and compound-nuclear processes using

$$\Gamma_{\lambda,\gamma i} = [\Gamma_{\lambda,\gamma(\text{CN})i}^{1/2} \pm \Gamma_{\lambda,\gamma(\text{val})i}^{1/2}]^2 \quad (15)$$

and after taking into account the sign correlation of the valence radiation widths, one finally arrives at four possible values of the resonance radiation width for the  $i$ th transition. Division by the spectral fraction  $f_{\gamma,i}$  gives an estimate of the total radiation width. If our hypothesis is correct, there should be for all transitions a common pair of values of the reduced neutron width and the total radiation width.

The valence radiation width is fully correlated with the reduced neutron width of the level [61], as well as with the final-state spectroscopic factor, and hence may be calculated accurately. The method used for this calculation is that described for discrete  $\mathcal{R}$ -matrix levels in Ref. [2]. In the current case, the  $s$ -wave  $\mathcal{R}$ -matrix single-particle state is calculated with a boundary condition at the channel radius appropriate to the thermal-neutron energy and placed at the binding energy of  $-29$  keV by adjustment of the potential depth. The ratio of the radiation width to neutron width for the  $\mathcal{R}$ -matrix single-particle state at thermal-neutron energy is then calculated and multiplied by  $\Gamma_n(\text{th})$  for the actual level to obtain the required valence radiation width.

For the 10.83-MeV transition to the ground state, the results of this analysis give two branches with very high values of  $\Gamma_{\lambda,(\text{tot})}$  ( $\sim 10$  eV) and one with low values ( $\sim 23$ – $230$  meV). The fourth branch lies in the range 1374 meV (for  $\gamma_{\lambda(n)}^2 = 49$  keV) to 298 meV (for  $\gamma_{\lambda(n)}^2 = 53$  keV). This branch [shown in Fig. 6(b)] is used as the only one in reasonable agreement with the  $M1$  analysis presented in Sec. V. The results for two other  $E1$  transitions for which sufficient data are available are also shown in Fig. 6(b) as a plot of

$\Gamma_{\lambda,(\text{tot})}$  vs  $\gamma_{\lambda(n)}^2$ . There is a considerable uncertainty in the analysis of the 4509-keV transition to the 6324-keV state. The assumption that the  $p$ -state admixture in this state is from the  $1p_{3/2}$  configuration gives high values of  $\Gamma_{\lambda,(\text{tot})}$ , generally well over 1 eV. Different behavior is obtained for the assumption of  $0p_{1/2}$  configuration. One branch runs from 540 meV (for  $\gamma_{\lambda(n)}^2 = 49$  keV) to 575 meV (for  $\gamma_{\lambda(n)}^2 = 53$  keV) as shown in Fig. 6(b). A second branch is very close, running from 620 to 660 meV, while the remaining two lie around 2 eV. The 1681-keV transition to the 9152-keV final state has very little contribution from the  $-131$ -keV level. Consequently, there are only two branches, one in the region  $\Gamma_{\lambda,\gamma(\text{tot})} \sim 570$  meV [as shown in Fig. 6(b)], the other at  $\sim 80$  meV.

The direct process can be included in the analysis of the  $M1$  transitions to the  $J^\pi = \frac{1}{2}^+, \frac{3}{2}^+$  final states in exactly the same way as was done for the  $E1$  transitions. The result is shown in Fig. 6(c), again exhibiting convergence close to a total radiation width of 550 meV and a reduced neutron width of 51 keV.

The sources of error in the above analysis are varied and complex. There are uncertainties of  $\sim 1$ – $4$  % in the measurement of the thermal-neutron-capture cross sections,  $\sim 20$ % in the  $(d,p)$  spectroscopic factors, and  $\sim 10$ % in the spectral abundances in the  $^{14}\text{C}(p,\gamma)$  reaction. These uncertainties, especially those in the spectroscopic factors, do not always translate directly into uncertainties on the final results. From a  $\chi^2$  analysis of all ten transitions that can yield information on the total radiation width, final values of  $\Gamma_{\lambda,\gamma(\text{tot})} = 565 \pm 24$  meV, and  $\gamma_{\lambda(n)}^2 = 51.6 \pm 0.3$  keV are obtained. Presented in Table IX(a) for  $E1$  and in Table IX(b) for  $M1$  transitions are our assessments of total, neutron valence, and compound-nuclear partial radiation widths. From our value of the total radiation width and the result from Refs. [33] for  $\Gamma_p \Gamma_{\gamma,\text{tot}} / \Gamma$ , the proton width of the  $-29$ -keV level is found to be to be  $\Gamma_p = 177 \pm 25$  meV, which is in agreement with the value given in Table V.

The assumption (discussed at the end of Sec. III) that the  $-131$ -keV level does not have positive parity weakens the above analysis. With a value of 55 keV for the reduced neutron width of the  $-29$ -keV level and no contribution from the  $-131$ -keV level, the optimum values of the total radiation width deduced from the various transitions range from 180 to 870 meV. In particular, there is no common value of the total radiation width as shown in Fig. 6 for the positive-parity assumption. This failure to converge strengthens the arguments in favor of  $J^\pi = \frac{3}{2}^+$  for the  $-131$ -keV level.

The strength of the compound-nuclear (CN) component of the radiation requires some comment. It appears from Table IX that the CN radiation width for the 10.83-MeV transition to the ground state is  $\sim 3.0$  eV. At this energy the  $E1$  radiative width could be substantially affected by the giant-dipole resonance. Using the formula of Brink [66], the radiative strength function  $\Gamma_\gamma/D$  is  $\sim 3 \times 10^{-6}$  at this  $\gamma$ -ray energy, if the energy of the giant-dipole resonance is taken as 20 MeV and its width as 4 MeV. The level spacing  $D$  for  $J^\pi = \frac{3}{2}^-$  levels at this excitation energy appears to be  $\sim 0.5$  MeV (see Table VII), indicating an expected  $\Gamma_\gamma$  of  $\sim 1.5$  eV. For the 4509-keV transition, the giant-dipole model gives  $\Gamma_\gamma \sim 25$  meV, which can be compared with the

TABLE IX. Valence and compound-nuclear radiation widths for  $E1$  and  $M1$  transitions from the  $-29$  keV resonance deduced from the  $^{14}\text{C}(p, \gamma)$  data and calculated neutron valence widths.

$E_f$ (keV)	$J^\pi$	$E_\gamma$ (keV)	Branching <sup>a</sup> (%)	$\Gamma_\gamma^b$ (meV)	$\Gamma_{\gamma,\text{val}}^c$ (meV)	$\Gamma_{\gamma,\text{CN}}^d$ (meV)	$\Gamma_{\gamma,\text{CN}}^e$ (meV)
(a) $E1$ transitions							
0	$\frac{1}{2}^-$	10 829	44 4	249	1469	3027	2928
6324 <sup>f</sup>	$\frac{3}{2}^-$	4509	6.8 7	38	27	131	123
9152	$\frac{3}{2}^-$	1681	2.9 4	16	2.7	5.7	5.8
(b) $M1$ transitions							
5270	$\frac{5}{2}^+$	5562	6.0 6	25		25	25
5299	$\frac{1}{2}^+$	5533	17.3 20	73	0.34	83	87
7155	$\frac{5}{2}^+$	3678	8.9 9	37		37	52
7300	$\frac{3}{2}^+$	3532	7.0 7	29	18	1	11
8312	$\frac{1}{2}^+$	2520	4.7 5	20	7	3	8
9155	$\frac{5}{2}^+$	1678	4 <sup>g</sup>	17		17	27

<sup>a</sup>From  $(p, \gamma)$  spectrum of Ref. [33].

<sup>b</sup>From total radiation width and branching.

<sup>c</sup>Calculated from reduced neutron width.

<sup>d</sup>From partial radiation width and valence width.

<sup>e</sup>From thermal-neutron cross section and calculated direct capture.

<sup>f</sup>Single-particle  $1p_{3/2}$  character assumed.

<sup>g</sup>Görres *et al.* [33] give a value of (2.1 4)% for this branch compared to 4% obtained earlier by Siefken, Cockburn, and Krone [30]. We use the latter value in our analysis because it is in better agreement with the (unpublished) datum of Beukens [32]. The branchings obtained by Beukens have been adopted in Table 15.5 of Ref. [41].

CN value of 131 meV. For the 1681-keV transition, the model value is  $\sim 0.5$  meV compared with the CN value of 5.7 meV. It is well-known that for low-energy transitions the Brink formula tends to underestimate the radiation width. The semiempirical Cameron formula [67] gives an expected value of  $\sim 5$  meV for the 1681-keV transition. Thus, the CN radiation widths given in Table VII are in complete accord with conventional expectations.

Less is known about the expected strength of the compound-nuclear  $M1$  transitions. Mottelson [68] has proposed a correlated spin-flip mechanism giving rise to a giant resonance analogous to the  $E1$  case. Estimates of the energy of the  $M1$  giant resonance and its strength are given by Bohr and Mottelson [69]. The experimental situation has been summarized by Raman, Fagg, and Hicks [70]. With a giant-resonance energy of 14 MeV, which is estimated to be appropriate for the nuclei at the upper end of the  $0p$  shell, and a Lorentzian spreading of the strength with half-width of 2 MeV into the CN states, partial radiation widths of 50, 8, and 0.4 meV are expected for the final states at about 5.3, 7.3, and 9.2 MeV, respectively. These estimates are in reasonable agreement with the extracted values of the CN widths of the lower states [see Table VII(b)], but that for the 9155-keV state is almost two orders of magnitude too short.

## VII. CONCLUSIONS

The thermal-neutron-capture cross section of  $\sim 80$  mb for  $^{14}\text{N}$  would seem, at first sight, to be typical of off-resonance capture by a light nucleus; this  $(n, \gamma)$  reaction, from our previous experience, might be expected to be almost entirely direct in nature. In fact, this reaction turns out to have one of the richest mixtures of resonant and off-resonant features in

neutron capture. Furthermore, it is anomalous in having a greater cross section for  $M1$  than  $E1$  transitions. The deceptively small total  $E1$  capture cross section ( $\sim 26$  mb) is a result of largely destructive interference in a few transitions between a complex compound-nuclear contribution from a relatively close bound level, a valence contribution from the same level, and a potential-capture contribution. The first two contributions are roughly commensurate for the principal transitions in the  $E1$  primary capture process, and potential capture also plays a significant role. The compound-nuclear contribution on its own would give a total capture cross section for  $E1$  transitions of  $\sim 475$  mb, while the valence contribution would be  $\sim 225$  mb. Potential capture alone would amount to  $\sim 284$  mb. These components interfere with each other. Our analysis of  $M1$  transitions suggests that a direct process plays a modest role here, but it does not grossly distort the spectrum from that which would result from resonance compound-nuclear capture alone. The magnitude of the latter is largely in agreement with the theory of the  $M1$  giant resonance.

The role of the bound level in the capture process has been established quantitatively from its observation as a resonance in the  $(p, \gamma)$  reaction, and from the behavior of the neutron total cross section at epithermal neutron energies. From these data, the reduced neutron width of this bound level has been deduced and also its total and partial  $\gamma$  radiation widths. Although the error bounds on the determination of the total radiation width from the  $(p, \gamma)$  data are very wide, it has been possible to establish its value (and hence the partial widths) much more precisely by comparing the proton-resonance spectrum with the thermal-neutron spectrum. To this end, our theoretical estimates of the valence

partial radiation widths were used together with the thermal-neutron direct-capture cross sections. The consensus of our analysis for several transitions establishes that the resonance total radiation width is  $\sim 565$  meV and proves the important role of the valence neutron capture mechanism in this resonance. The significance of this indirect detection of valence neutron capture is that it constitutes the first observation of this process in a resonance that has not been initiated by the neutron. In other words, the neutron valence radiation width amplitude, while a significant fraction of the compound-nuclear radiation amplitude, is not correlated with the entrance channel width. The reduced neutron width of the level is 51.6 keV; this value corresponds in neutron spectroscopy language to a  $\Gamma_n^0$  (neutron width reduced to 1 eV energy)

value of 85 eV. This is not a particularly strong neutron resonance level. However, its properties are such that this resonance fully accounts for the  $^{14}\text{N}$  thermal-neutron capture  $\gamma$ -ray spectrum.

#### ACKNOWLEDGMENTS

We thank G. M. Hale (Los Alamos) for making available preliminary results [part (b) of Table V] from his  $\mathcal{R}$ -matrix analysis of existing resonance data. The current work was sponsored by the U.S. Department of Energy under Contract No. W-7405-eng-36 with the University of California (Los Alamos) and Contract No. DE-AC05-96OR22464 with Lockheed Martin Energy Research Corporation (Oak Ridge).

- 
- [1] A. M. Lane and J. E. Lynn, Nucl. Phys. **17**, 563 (1960); **17**, 586 (1960).
- [2] S. Raman, R. F. Carlton, J. C. Wells, E. T. Journey, and J. E. Lynn, Phys. Rev. C **32**, 18 (1985).
- [3] S. Raman and J. E. Lynn, in *Proceedings of the Fourth International Symposium on Neutron Induced Reactions*, Smolenice, Czechoslovakia, 1985, edited by J. Krištiak and E. Běťák (VEDA, Bratislava, 1986), p. 253.
- [4] J. E. Lynn, S. Kahane, and S. Raman, Phys. Rev. C **35**, 26 (1987).
- [5] S. Raman, S. Kahane, and J. E. Lynn, in *Proceedings of the Sixth International Symposium on Capture Gamma-ray Spectroscopy*, Leuven, Belgium, 1987, edited by H. Abrahams and P. Van Assche (Institute of Physics, Bristol, 1988), p. S223.
- [6] S. Kahane, J. E. Lynn, and S. Raman, Phys. Rev. C **36**, 533 (1987); S. Raman, S. Kahane, R. M. Moon, J. A. Fernandez-Baca, J. L. Zarestky, J. E. Lynn, and J. W. Richardson, Jr., *ibid.* **39**, 1297 (1989); S. Raman, J. A. Fernandez-Baca, R. M. Moon, and J. E. Lynn, *ibid.* **44**, 518 (1991).
- [7] S. Raman, S. Kahane, and J. E. Lynn, in *Proceedings of the International Conference on Nuclear Data for Science and Technology*, Mito, Japan, 1988, edited by S. Igarasi (Saikon, Tokyo, 1988), p. 645.
- [8] S. Raman, M. Igashira, Y. Dozono, H. Kitazawa, M. Mizumoto, and J. E. Lynn, Phys. Rev. C **41**, 458 (1990).
- [9] J. E. Lynn, E. T. Journey, and S. Raman, Phys. Rev. C **44**, 764 (1991).
- [10] J. E. Lynn and S. Raman, in *Capture Gamma-Ray Spectroscopy*, edited by R. W. Hoff, AIP Conf. Proc. No. 238 (AIP, New York, 1991), p. 555.
- [11] T. A. Walkiewicz, S. Raman, E. T. Journey, J. W. Starner, and J. E. Lynn, Phys. Rev. C **45**, 1597 (1992).
- [12] S. Raman and J. E. Lynn, in *Beijing International Symposium on Fast Neutron Physics*, Beijing, China, 1991, edited by Sun Zuxun, Tang Hongqing, Xu Jincheng, and Zhang Jingshang (World Scientific, Singapore, 1992), p. 107.
- [13] S. Raman, E. T. Journey, J. W. Starner, and J. E. Lynn, Phys. Rev. C **46**, 972 (1992).
- [14] M. C. Moxon, J. A. Harvey, S. Raman, J. E. Lynn, and W. Ratynski, Phys. Rev. C **48**, 553 (1993).
- [15] S. Raman, E. K. Warburton, E. T. Journey, J. W. Starner, and J. E. Lynn, Phys. Rev. C **53**, 616 (1996).
- [16] H. T. Motz, R. E. Carter, and W. D. Barfield, in *Pile Neutron Research* (International Atomic Energy Agency, Vienna, Austria, 1962), p. 15.
- [17] G. E. Thomas, D. E. Blatchley, and L. M. Bollinger, Nucl. Instrum. Methods **56**, 325 (1967); G. D. Loper and G. E. Thomas, *ibid.* **105**, 453 (1972); G. E. Thomas and R. H. Pehl, *ibid.* **121**, 65 (1974).
- [18] R. C. Greenwood, Phys. Lett. **27B**, 274 (1968); R. C. Greenwood and R. G. Helmer, Nucl. Instrum. Methods **121**, 385 (1974); R. C. Greenwood, R. G. Helmer, R. J. Gehrke, and R. E. Chrien, in *Atomic Masses and Fundamental Constants 6*, edited by J. A. Nolen, Jr. and W. Benenson (Plenum, New York, 1980), p. 219; R. G. Helmer, R. C. Greenwood, and R. J. Gehrke, Nucl. Instrum. Methods **159**, 465 (1980); R. C. Greenwood and R. E. Chrien, *ibid.* **175**, 515 (1980).
- [19] L. Jonsson and R. Hardell, in *Proceedings of the International Symposium on Neutron Capture Gamma-Ray Spectroscopy*, Studsvik, edited by N. Ryde (International Atomic Energy Agency, Vienna, Austria, 1969), p. 199.
- [20] D. Bellman, Atom Kernenergie **17**, 145 (1971).
- [21] A. F. M. Ishaq, A. M. Khan, M. Anwar-ul-Islam, and M. R. Najam, Nucl. Instrum. Methods **121**, 193 (1974).
- [22] B. Krusche, K. P. Lieb, H. Daniel, T. von Egidy, G. Barreau, H. G. Börner, R. Brissot, C. Hofmeyr, and R. Rascher, Nucl. Phys. **A386**, 245 (1982). The  $\gamma$ -ray energies listed in Table 2 of this paper are uncorrected for recoil even though the footnote states otherwise.
- [23] S. Raman, E. T. Journey, D. A. Outlaw, and I. S. Towner, Phys. Rev. C **27**, 1188 (1983).
- [24] T. J. Kennett, W. V. Prestwich, R. J. Tervo, and J. S. Tsai, Nucl. Instrum. Methods Phys. Res. A **215**, 159 (1983); T. J. Kennett, W. V. Prestwich, and J. S. Tsai, *ibid.* **249**, 366 (1986).
- [25] M. A. Islam, T. J. Kennett, and W. V. Prestwich, Nucl. Instrum. Methods Phys. Res. A **287**, 460 (1990).
- [26] G. A. Bartholomew, F. Brown, H. E. Gove, A. E. Litherland, and E. B. Paul, Can. J. Phys. **33**, 441 (1955).
- [27] A. J. Ferguson and H. E. Gove, Can. J. Phys. **37**, 660 (1959).
- [28] D. F. Hebbard and D. N. F. Dunbar, Phys. Rev. **115**, 624 (1959).
- [29] D. F. Hebbard, Nucl. Phys. **19**, 511 (1960).

- [30] H. E. Siefken, P. M. Cockburn, and R. W. Krone, *Nucl. Phys.* **A128**, 162 (1969).
- [31] R. P. Beukens, T. E. Drake, and A. E. Litherland, *Phys. Lett.* **56B**, 253 (1975).
- [32] R. P. Beukens, Ph.D. thesis, University of Toronto, 1976.
- [33] J. Görres, S. Graff, M. Wiescher, R. E. Azuma, C. A. Barnes, H. W. Becker, and T. R. Wang, *Nucl. Phys.* **A517**, 329 (1990).
- [34] A. H. Wapstra, *Nucl. Instrum. Methods Phys. Res. A* **292**, 671 (1990). The values listed here are consistent with those given in Ref. [35].
- [35] G. Audi and A. H. Wapstra, *Nucl. Phys.* **A565**, 1 (1995).
- [36] S. Raman, *Phys. Rev. C* **2**, 2176 (1970).
- [37] G. R. Meredith and R. A. Meyer, *Nucl. Phys.* **A142**, 513 (1970).
- [38] S. Raman, in *Proceedings of the Fourth International Symposium on Neutron-Capture Gamma-ray Spectroscopy and Related Topics*, Grenoble, France, 1981, edited by T. von Egidy, F. Gönnenwein, and B. Maier (Institute of Physics, Bristol, 1982), p. 357.
- [39] E. T. Journey, *Phys. Rev. C* **25**, 2810 (1982).
- [40] S. F. Mughabghab, M. A. Lone, and B. C. Robertson, *Phys. Rev. C* **26**, 2698 (1982).
- [41] S. F. Mughabghab, M. Divadeenam, and N. E. Holden, *Neutron Cross-Sections* (Academic, New York, 1981), Vol. 1, Part A, p. 1-1.
- [42] F. Ajzenberg-Selove, *Nucl. Phys.* **A449**, 1 (1986); **A523**, 1 (1991).
- [43] F. DiFilippo, V. Natarajan, M. Bradley, F. Palmer, and D. E. Pritchard, *Phys. Scr.* **T59**, 144 (1995).
- [44] S. Raman, E. T. Journey, J. W. Starnier, A. Kuronen, J. Keinonen, K. Nordlund, and D. J. Millener, *Phys. Rev. C* **50**, 682 (1994).
- [45] G. W. Phillips and W. W. Jacobs, *Phys. Rev.* **184**, 1052 (1969).
- [46] A. Amokrane, M. Allab, H. Beaumevieille, B. Faid, O. Bersillon, B. Chambon, D. Drain, and J. L. Vidal, *Phys. Rev. C* **6**, 1934 (1972).
- [47] W. Kretschmer, G. Pröbstle, and W. Stach, *Nucl. Phys.* **A333**, 13 (1980).
- [48] L. Koester, K. Knopf, and W. Waschkowski, *Z. Phys. A* **277**, 77 (1976).
- [49] W. D. Roseborough, J. J. G. McCue, W. M. Preston, and C. Goodman, *Phys. Rev.* **83**, 1133 (1951).
- [50] R. M. Sanders, *Phys. Rev.* **104**, 1434 (1956).
- [51] W. R. Harris and J. C. Armstrong, *Phys. Rev.* **171**, 1230 (1968).
- [52] P. A. Moldauer, *Nucl. Phys.* **47**, 65 (1963).
- [53] G. M. Hale, P. G. Young, and M. B. Chadwick, in *Proceedings of the International Conference on Nuclear Data for Science and Technology*, Gatlinburg, 1991, edited by J. K. Dickens (ANS, La Grange Park, 1994), p. 607; (private communication).
- [54] J. A. Harvey, N. W. Hill, N. M. Larson, and D. C. Larson, in *Proceedings of the Conference on Nuclear Data for Science and Technology*, Jülich, 1991, edited by S. M. Qaim (Springer, Berlin, 1992), p. 729; C. O. Beasley, Jr., N. M. Larson, J. A. Harvey, D. C. Larson, and G. M. Hale, in *Reactor Dosimetry*, edited by H. Farrar IV, E. P. Lippincott, J. G. Williams, and D. W. Vehar, ASTM Publication No. 04-012280-35 (ASTM, Philadelphia, 1994), p. 737.
- [55] A. M. Lane and R. G. Thomas, *Rev. Mod. Phys.* **30**, 257 (1958).
- [56] Š. Piskoř and W. Schäferlingová, *Nucl. Phys.* **A510**, 301 (1990).
- [57] G. C. Hanna, *Can. J. Phys.* **39**, 1784 (1961).
- [58] G. L. Morgan, *Nucl. Sci. Eng.* **70**, 163 (1979).
- [59] K. Brehm, H. W. Becker, C. Rolfs, H. P. Trautvetter, F. Käppler, and W. Ratynski, *Z. Phys. A* **330**, 167 (1988).
- [60] P. E. Koehler and H. A. O'Brien, *Phys. Rev. C* **39**, 1655 (1989); P. E. Koehler, *ibid.* **48**, 439 (1993).
- [61] J. E. Lynn, *The Theory of Neutron Resonance Reactions* (Oxford University Press, Oxford, 1968), p. 305.
- [62] J. Cugnon and C. Mahaux, *Ann. Phys. (N.Y.)* **94**, 128 (1975).
- [63] Y. K. Ho and M. A. Lone, *Nucl. Phys.* **A406**, 18 (1983).
- [64] J. M. Blatt and V. F. Weisskopf, *Theoretical Nuclear Physics* (Wiley, New York, 1952), p. 627.
- [65] E. K. Warburton, J. W. Olness, and D. E. Alburger, *Phys. Rev.* **140**, B1202 (1965).
- [66] D. M. Brink, Ph.D. thesis, Oxford, 1955.
- [67] A. G. W. Cameron, *Can. J. Phys.* **35**, 666 (1957).
- [68] B. R. Mottelson, in *Proceedings of the International Conference on Nuclear Structure*, edited by J. Sanada [*J. Phys. Soc. Jpn.* **24**, 87 (1968)].
- [69] A. Bohr and B. Mottelson, *Nuclear Structure* (Benjamin, Reading, 1975), Vol. II, p. 636.
- [70] S. Raman, L. W. Fagg, and R. S. Hicks, in *Electric and Magnetic Giant Resonances in Nuclei*, edited by J. Speth (World Scientific, Singapore, 1991), p. 355.